Applied Catalysis B: Environmental 321 (2023) 122047

Contents lists available at ScienceDirect

Applied Catalysis B: Environmental

journal homepage: www.elsevier.com/locate/apcatb

Finely regulating methanol concentration to control the alkylation depth in methanol aromatization for optimizing product distribution

Liangliang Zhang [a], Tingjun Fu [a,*], Kun Ren [a], Yating Han [a], Ran Wang [a], Guowu Zhan [b,*], Zhong Li [a,*]

[a] State Key Laboratory of Clean and Efficient Coal Utilization, Taiyuan University of Technology, Taiyuan 030024, Shanxi, China
[b] College of Chemical Engineering, Huaqiao University, Xiamen 361021, Fujian, China

ARTICLE INFO

Keywords:
MTA
Methanol involvement
Alkylation
Product distribution
Dual bed

ABSTRACT

Uncontrollable alkylation in methanol to aromatics severely restricts the light aromatic selectivity and catalytic stability. Herein, we proposed a new strategy to control the alkylation depth by precisely regulating methanol concentration in alkylation environment. Firstly, the high Si/Al ratio ZSM-5 (HZ) was packed over Zn doped low Si/Al ratio ZSM-5 (Zn/LZ) to form dual bed to inhibit deep alkylation for high catalytic stability and BTX selectivity. Secondly, part of methanol was introduced into lower Zn/LZ bed to promote methyl-cyclopentene alkylation for aromatic production and product optimization. After such regulation, toluene selectivity in aromatics decreased from 27.9% to 20.8% accompanied by an increase in xylene selectivity from 37.1% to 44.0%. BTX selectivity in aromatics also improved to 66.7% with 97.5 h of catalyst lifetime, much higher than 50.0% and 20 h of the single Zn/LZ bed. This work realized stable light aromatic production from methanol by controlling the microscopic reaction routes.

1. Introduction

Benzene, toluene, and xylene (BTX) are important chemical raw materials, which are widely used as synthetic monomer or solvent in medicine, pesticide, plasthetics and other industries [1]. At present, the production of these light aromatics mainly depends on the non-renewable petroleum resources. However, with the unabatedly increase of greenhouse gas emissions and the depletion of petroleum resources in the world, the fossil-fuel-derived aromatic production, such as the process of catalytic reforming in refineries, steam cracking of naphtha and aromatization of light hydrocarbons, is gradually becoming unpopular [2–5]. In contrast, methanol to aromatic (MTA) shows greater development potential for aromatic production because that the production of methanol can achieve zero or negative CO_2 emissions by using renewable feedstock and new energy resources, such as wind energy, solar energy, etc [6]. However, because of the complex distribution of products and the rapid coke-induced inactivation of acid zeolite catalysts, a large amount of energy consumption is still needed to regenerate the spent catalysts and purify the products, which causes waste of carbon resources and makes the MTA unsustainable [7]. Thus, the improvement of target product selectivity and catalytic stability are urgently needed to achieve high efficiency and low energy consumption of MTA technology.

The acidic ZSM-5 zeolite was the star catalyst for MTA, while it usually encounters a fast coke-induced inactivation and poor aromatic selectivity due to the intense complex reaction over strong acid sites and the serious diffusional limitation of micropore [8–11]. It is generally believed that methanol is firstly dehydrated into light olefins via dimethyl ether or acetaldehyde, and then aromatics are generated by subsequent polymerization, cyclization, and hydrogen transfer reaction [12–15]. In this reaction network, methanol was not only involved in the generation of light olefins, it also participated in the hydrogen transfer reaction with olefins in the form of formaldehyde [14]. The strong hydrogen transfer reaction among olefins or between olefins and methanol that occurred on Brønsted acid sites inevitably reduces the selectivity of aromatics in the final products [16].

Optimizing the pore and surface acid properties of the ZSM-5 catalyst can improve aromatic selectivity and catalytic stability. Reducing the crystal particle size or introducing the mesoporous into ZSM-5 zeolite are practical strategies to promote the reactant diffusion and increase the accessibility of acid active sites, which can improve the aromatization performance and prolong the catalytic life [17–20]. Constructing

* Corresponding authors.
E-mail addresses: futingjun@tyut.edu.cn (T. Fu), gwzhan@hqu.edu.cn (G. Zhan), lizhong@tyut.edu.cn (Z. Li).

https://doi.org/10.1016/j.apcatb.2022.122047
Received 4 August 2022; Received in revised form 29 September 2022; Accepted 3 October 2022
Available online 4 October 2022

the ZSM-5 catalyst with short b-axis can signally prolong the catalytic lifetime from dozens of hours to more than hundred hours, and the aromatic yield could exceed 50.0% due to the high-efficiency diffusion of aromatic molecules passing through straight channels [21–23]. Decreasing Si/Al ratio and increasing acid density can promote aromatization, but enrich the production of low carbon alkanes and accelerate catalyst deactivation [24]. More crucially, most of the generated aromatic products were heavy aromatics because of the strong alkylation reaction on the external surface [23].

On the other hand, doping the metal species, such as Zn [25–27], Ga [28,29] and Ni [30,31] etc, can convert Brønsted acid sites of ZSM-5 into metal-Lewis acid sites, which greatly inhibits hydrogen transfer reaction and enhances the dehydrogenation reaction, and finally promotes the generation of aromatics. Further passivating the surface acid sites of ZSM-5 by the modification of Si, Mg and P species can effectively inhibit surface alkylation and promote the production of light aromatics [16, 32–34]. However, the total aromatics selectivity and catalytic stability were observably reduced due to the inevitable decrease of acid density and increase of diffusion resistance in these modified samples. Therefore, how to simultaneously obtain high light aromatic selectivity and high catalytic stability remains a huge challenge.

As discussed above, most of the current studies are focused on the modification of acid properties or pore structure of ZSM-5 catalyst, which has limited effect on the improvement of aromatization performance. It is worth noting that methanol not only acts as a reactant to produce olefins and aromatics, but also participates in the alkylation reaction of aromatics as an active alkylation agent [35,36]. Especially on the external surface of ZSM-5, BTX diffused from the microporous channel further reacted to form trimethylbenzene and tetramethylbenzene due to the abundant external surface acids and high methanol concentration [37]. The deep alkylation process not only caused the decrease of light aromatic selectivity, but also inevitably promoted the formation of coke deposition and accelerated catalyst deactivation [38,39]. Chen et al. obviously inhibited the dealkylation process and improved the selectivity of xylene by dispersing methanol into a fluidized bed reactor [40]. Thus, it is necessary to fully consider the important role of methanol in aromatic alkylation process for the optimization of product distribution and the improvement of catalytic stability in MTA.

In this work, two strategies were proposed to control the depth of alkylation reaction by adjusting the methanol involvement for the high aromatization performance of ZSM-5 zeolite in MTA. On one hand, high Si/Al ratio ZSM-5 (HZ) were packed over the Zn doped low Si/Al ratio ZSM-5 (Zn/LZ) to pre-convert methanol and prevent excessive alkylation of aromatics. On the other hand, an extra drainage tube with the diameter of 3 mm was specifically buried into the catalyst bed to introduce part of methanol into the lower Zn/LZ bed to adjust the product distribution. As shown in Fig. 1, we respectively introduced the methanol into the six different locations along the axial direction of the reactor (three in upper HZ bed and three in lower Zn/LZ bed). The influence of methanol-imported position on aromatic alkylation process and aromatic distribution was carefully studied. Combined with the performance evaluation results, coke deposition analysis and in situ experiments, the influence of alkylation depth on the MTA process was studied. The results revealed that the stable and efficient aromatics production, especially for xylene, required moderate alkylation processes. The proposed dual ZSM-5 bed with stratified methanol feed showed a more excellent catalytic stability and higher light aromatic selectivity with a high proportion of xylene than that of single Zn/LZ bed. This work offered a novel approach for regulating product distribution in MTA reaction with high catalytic stability of ZSM-5.

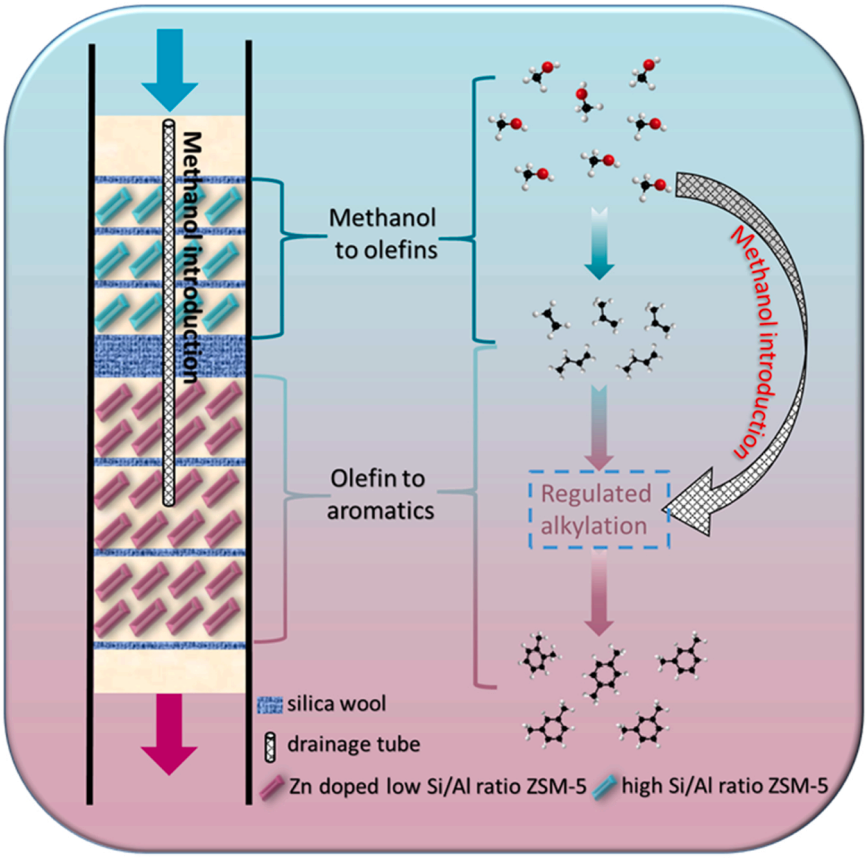

Fig. 1. The diagram of regulating methanol involvement to control the alkylation depth for optimizing product distribution in methanol aromatization.

2. Experiment

2.1. Catalyst preparation

Nanocrystalline ZSM-5 zeolites with high acid density and low acid density were successfully synthesized according to our previous papers [41]. For the ZSM-5 with low acid density, 108.0 g tetrapropylammonium hydroxide and 112.5 g tetraethyl orthosilicate were firstly mixed in a 500 ml three-necked flask and tardily heated at 80 °C. After constant stirring for 24 h, 0.8 g aluminum nitrate nonahydrate and 3.6 g sodium hydroxide were dissolved in 16.0 g and 20.0 g deionized water respectively. Then they were dropped into above mixture using a peristaltic pump with the rotate speed of 25 r min^{-1}. The final mixture was further stirring for another 5.5 h at 80 °C to get an aluminosilicate gel with the mole material composition of 60 SiO_2: 0.12 Al_2O_3:15 TPAOH: 5 Na_2O: 718 H_2O. The crystallization process of above aluminosilicate gel was carried out at 170 °C using a stainless steel Teflon-lined autoclave. After continuous heating for 24 h, the crystal compound was cooled and centrifuged to obtain solid zeolite. Subsequently, the solid samples were washed with deionized water until the PH of filter liquor attained to 7. The waterish samples were dried overnight at 100 °C and then calcined at 550 °C for 6 h to remove the residual organic templates. To obtain the acidic ZSM-5, the Na-ZSM-5 was firstly translated into NH_4-ZSM-5 by ion exchanges with 0.8 M NH_4Cl solution at 80 °C, which was repeated three times and the duration of each time was 3 h. After continuity calcining the NH_4-ZSM-5 for 6 h at 550 °C, the H-ZSM-5 was finally obtained. Finally, the H-ZSM-5 with low acid density was acquired and denoted as HZ.

For the ZSM-5 with high acid density, the Na-ZSM-5 was also synthesized by increasing the additive amount of aluminum nitrate nonahydrate to 6.8 g based on above methods. The mole material composition of aluminosilicate gel was correspondingly tuned to 60 SiO_2: 1 Al_2O_3: 15 TPAOH: 5 Na_2O: 718 H_2O. The according H-ZSM-5 with high acid density was denoted as LZ. Specially, in order to obtain higher dehydrogenation performance for aromatization process, the acid property of LZ was further adjusted by doping 4 wt% Zn species via an incipient wetness impregnation method with zinc nitrate hexahydrate and further calcined at 500 °C for 4 h. The final Zn doped ZSM-5 catalyst was denoted as Zn/LZ.

2.2. Catalysts characterization

The crystallinity of the synthesized ZSM-5 zeolites were analyzed by the powder X-ray diffraction (XRD) patterns recorded on a Rigaku D/Max 2500 diffractometer equipped with Cu Kα (λ = 1.54439 Å) radiation. The 2θ range was 5–50° with a scanning speed of 8° min^{-1}. A JEM-2100 F transmission electron microscopy (TEM) was adopted to characterize the morphologies of fresh and spent ZSM-5 catalysts. Before the test, the samples were scattered in ethanol firstly and then dropped onto the carbon-coated copper grids. The structural properties of all fresh and spent ZSM-5 catalysts were analyzed by N_2 adsorption and desorption isotherms which were carried out at − 196 °C using a Beishide 3 H-2000PS2 instrument. The impurities adsorbed in catalysts were beforehand removed by pretreating the samples at 250 °C for 4 h under vacuum condition.

The actual Si/Al ratio of the obtained catalyst and the Zn doped amount in Zn/LZ were measured by X-ray Fluorescence Spectrometer (XRF). The strength and amount of acid sites of the ZSM-5 catalysts were tested by temperature-programmed desorption of ammonia (NH_3-TPD) carried out on a Micromeritics Autochem II 2920 analyzer equipped a thermal conductivity detector. Typically, the sample was pretreated at 550 °C for 60 min in a He flow to remove the absorbed impurities. 5 v% ammonia-helium was selected as the treatment gas and fed into U-type tube when the temperature cooled to 120 °C. After attaining the adsorption equilibrium and the based-line stabilization, the NH_3-TPD curves were recorded at 120–650 °C with a rate of 10 °C min^{-1}.

The Brønsted or Lewis acid sites on ZSM-5 catalysts were also determined by pyridine adsorption-desorption infrared spectra, which were recorded on a Bruker Tensor II FTIR spectrometer equipped with a vacuum chamber. The self-supporting sample wafer with 6.5 mm radius was pretreated at 400 °C for 90 min in a vacuum (10^{-2} Pa) to pump out the absorbed impurities. After that, pyridine was fed in at room temperature and maintained for 30 min to ensure the adequate adsorption of pyridine on acidic sites. The pyridine desorption curves were recorded at room temperature after continuing the desorption of pyridine at 400 °C for 1 h. Based on the obtained spectra, the concentration of the Brønsted sites ($C_{(B)}$) and Lewis sites ($C_{(L)}$) were calculated using the following equation [42]:

$$C_{(B)} = \frac{1.88 \times IA \times R^2}{W}$$

$$C_{(L)} = \frac{1.42 \times IA \times R^2}{W}$$

wherein, IA is the integral area of the selected vibration bands, 1540 cm^{-1} for Brønsted sites and 1450 cm^{-1} for Lewis sites; R (6.5 mm) and W (30 mg) are the radius and weight of the tested self-supporting wafer, respectively.

A STA449F3 thermogravimetric analyzer was adopted to conduct the thermal gravimeter analysis (TGA) to analyze the coke deposition amount on spent ZSM-5 catalysts. The TGA curves were recorded at the temperature of 30–750 °C at a heating rate of 10 °C min^{-1} under the air atmosphere with the flow rate of 30 ml min^{-1}. The internal coke amount was calculated by multiplying the lost microspore volume and the coke density (1.22 g cm^{-3}) according to previous literature reports [43–45]. Distinctly, the amount of external coke could be obtained by subtracting the internal coke content from the total coke content.

GC-MS analysis was carried out on Agilent 8890–5977B gas chromatograph-mass spectrometer equipped with a HP-5MS UI capillary column (30 m, 0.25 mm i.d., 0.25 μm film thickness). First, 10 mg used catalyst was dissolved in the 1 ml of 10 v% HF solution to remove the zeolite skeleton. Then 1 ml of methylene dichloride (CH_2Cl_2) was added to the above solution to extract the soluble organic species. The 1 μl extract was analyzed. During the reanalysis, the temperature was kept at 40 ℃ for 15 min firstly, and then heated to 300 °C at a rate of 5 °C min^{-1} and kept for 15 min.

The in situ diffuse-reflectance infrared fourier transform spectroscopy (DRIFTS) measurements about methanol reaction, propylene conversion and propylene-methanol co-reaction were performed on Bruker Tensor 27. Prior to the tests, the catalyst was pretreated at 450 °C for 60 min under nitrogen atmosphere. After reducing the temperature to 350 °C, the constant flow of 9 v% propylene/N_2 with the rate of 3 ml min^{-1} was entered into the in situ reaction chamber for propylene reaction. Methanol was carried into the chamber through bubbling method by propylene-nitrogen gas flow and nitrogen gas flow for propylene-methanol co-reaction and methanol reaction respectively. The spectrogram was recorded with time on stream from 1 min to 60 min. The final spectra were obtained by subtracting the background spectrum (obtained before the reactant was brought in) from the measured sample spectra.

Temperature-programmed desorption experiments were performed at Micromeritics Autochem II 2920 analyzer. Concretely, 0.1 g sample was packed in the into U-type tube and pretreated at 550 °C for 60 min under He atmosphere. Then, the adsorbate was fed after the temperature dropped to 100 °C. For methanol adsorption, methanol was introduced by the bubbling method using He as the carrier gas. 9 v% propylene/N_2 was selected as treatment gas for propylene adsorption, which also was used as the carrier gas to bubble methanol for propylene-methanol co-adsorption. The desorption was carried out by increasing the temperature to 600 °C with the ratio of 5 °C min^{-1} after the adsorption equilibrium and the based-line stabilization. The desorbed species were

monitored by an on-line MS analyzer (Hiden HPR-20 EGA). The m/e values of desorbed species were referred as : 2 for hydrogen, 12 for carbon monoxide, 16 for methane, 27 for ethylene (after subtracting fragment ion signal of m/e 27 from propene), 29 for propane, 30 for formaldehyde (after deducting the fragment ion signal of m/e 30 from methanol), 31 for methanol, 41 for propylene, 44 for acetaldehyde, (after deducting the fragment ion signal of m/e 44 from CO_2), 53 for butadiene, 67 for MCP and 91 for aromatics [46,47].

2.3. Performance evaluation

The methanol aromatization reaction was carried out in a fixed-bed reactor with 12 mm inner diameter. In order to inhibit aromatics alkylation, a dual ZSM-5 catalyst bed was designed by packing a certain amount of ZSM-5 with low acid density over another Zn doped ZSM-5 catalyst with high acid density. In detail, the upper stage of catalyst bed was packed with 0.6 g HZ catalysts which were divided into three layers. Then 0.9 g Zn/LZ catalysts were also divided into three layers and loaded at the lower stage. In order to further control the depth of alkylation and optimize the product selectivity, an extra drainage tube with the diameter of 3 mm was buried into the catalyst bed to introduce methanol into the appointed catalyst layer. Based on the location of "appointed catalyst layer", the corresponding evaluation modes were denoted as GU-i or GL-i ("i" = 1, 2, 3). "GU" and "GL" represented the upper HZ catalyst stage and lower Zn/LZ catalyst stage, respectively. The "i" indicated the sequence number of catalyst layer, which was numbered as 1, 2, and 3 from top to bottom in HZ or Zn/LZ catalyst stage. For example, GU-2 meant that methanol was guided into the second catalyst layer of the upper HZ catalyst bed. In addition, another extra drainage tube was buried into the catalyst bed to adjust the amount of methanol that entered into the lower bed, which was denoted as DGL-1 (Fig. 2). To highlight the control effect of alkylation depth, the Zn/LZ catalyst was specially evaluated at the single bed, and the corresponding mode was denoted as SL.

In the typical experiments, all ZSM-5 catalysts were pelletized, crushed, and sieved to 80–100 mesh, and further mixed with the same amount silica sand. The packed catalysts were activated at 450 °C for 1 h under the nitrogen atmosphere before reaction. The reactions were carried out at 430 °C under atmospheric pressure with a liquid weight hourly space velocity (WHSV) of 4 h^{-1}. A Zhongkehuifen GC-7820 gas chromatograph (GC) connected to a flame ionization detector (FID) and a thermal conductivity detector (TCD) was used to analyze the gaseous and aqueous products. A Shimadzu GC-2014 C equipped with a 50 m HP-PONA capillary column was chose to analyze the oil phase products cooled by a cold trap (temperature of −2 °C). The conversion of methanol and selectivity of hydrocarbon product were calculated based on the GC results.

The calculation formula about methanol conversion was:

$X_m = \frac{m_{inlet}-m_{out}}{m_{inlet}} \times 100\%$, m is the mass of methanol.

The calculation formula about the selectivity of hydrocarbon product was:

$S_i = \frac{n_i}{\sum n_i} \times 100\%$, n_i is the number of carbon in the product i.

The calculation formula about the yield of liquid hydrocarbons was:

$Y = \frac{m_{oil}}{m_{methanol}} \times 100\%$, m_{oil} is the quality of oil phase products obtained at a certain reaction stage and $m_{methanol}$ is the quality of inlet methanol at this stage.

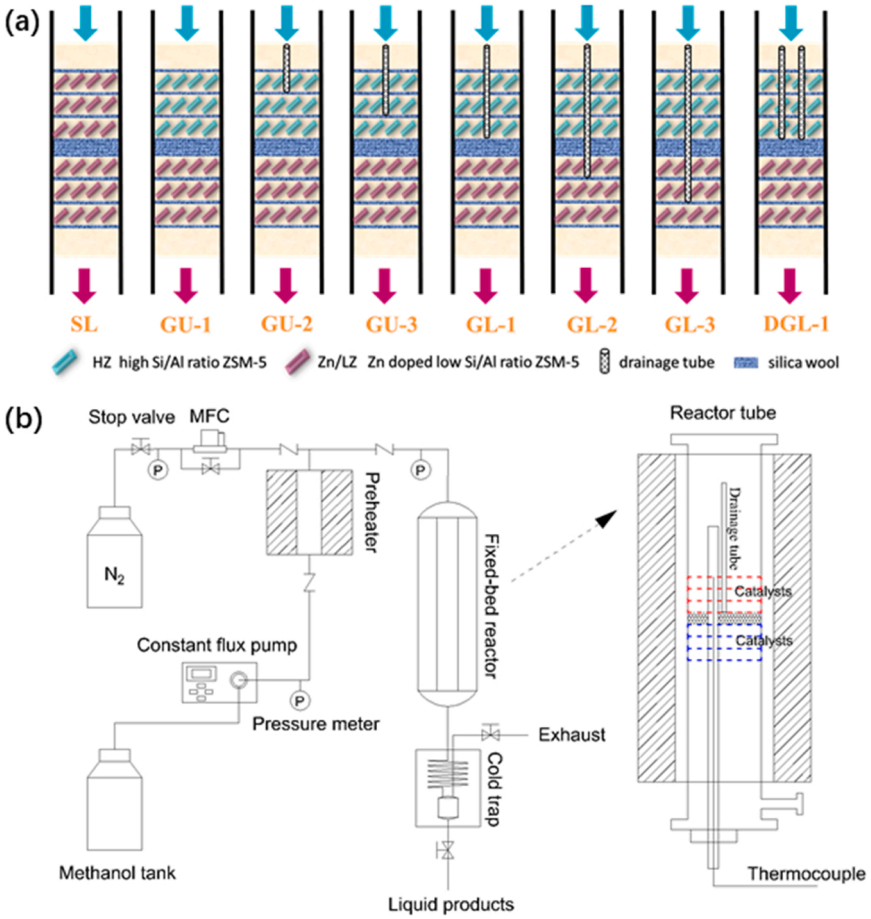

Fig. 2. The diagram of catalyst loading modes (a) and reaction evaluation equipment (b).

3. Results and discussion

3.1. Elementary structure properties of catalysts

The nano-size ZSM-5 zeolites were synthesized through the traditional hydrothermal method with a low H_2O/Si molar ratio of 11.9. And the acid density of ZSM-5 zeolite was adjusted by changing the amount of aluminum source. The XRF results revealed that the actual Si/Al ratio was 144 for HZ and 24 for LZ, respectively. And 3.9 wt% of Zn was found in the final Zn/LZ catalyst, which was close to the theoretical value. The XRD patterns of all synthesized samples presented typical diffraction patterns of MFI topology in Fig. 3a, which indicated that the ZSM-5 zeolites had been successfully prepared [41]. No additional picks related to the Zn species existed in the XRD pattern of Zn/LZ, suggesting that the introduced Zn species were highly dispersed on the external surface of Zn/LZ or in its channels [48]. Because of this, the specific surface area and pore volume of low Si/Al ratio ZSM-5 (LZ) obviously reduced from 366 cm^2 g^{-1} and 0.14 cm^3 g^{-1} to 322 cm^2 g^{-1} and 0.12 cm^3 g^{-1} after Zn deposition (Zn/LZ), respectively (Table 1, Fig. 3b and c). The TEM images of these ZSM-5 catalysts showed a typical coffin-like morphology and the size of them about 150 nm along the c axis (Fig. 3d-f). The smooth surface of Zn/LZ crystals proved once again that Zn species were highly dispersed.

Table 1
Textural properties of fresh catalysts.

Samples	Surface area (m^2 g^{-1})			Pore volume (cm^3 g^{-1})		
	S_{BET} [a]	S_{Micro} [b]	S_{Meso} [c]	V_{Total} [d]	V_{Micro} [e]	V_{Meso} [f]
HZ	342	290	52	0.54	0.14	0.40
LZ	366	292	74	0.44	0.14	0.30
Zn/LZ	322	258	64	0.44	0.12	0.32

[a] S_{BET} calculated by the BET method.
[b] S_{Micro} measured by the t-plot method.
[c] S_{Meso} calculated by the formula of $S_{Meso} = S_{Total} - S_{Micro}$.
[d] V_{Total} determined by N_2 adsorption volume at $P/P_0 = 0.9$.
[e] V_{Micro} measured by the t-plot method.
[f] V_{Meso} calculated by the formula of $V_{Meso} = V_{Total} - V_{Micro}$.

The acidity of the synthesized acidic ZSM-5 zeolites was

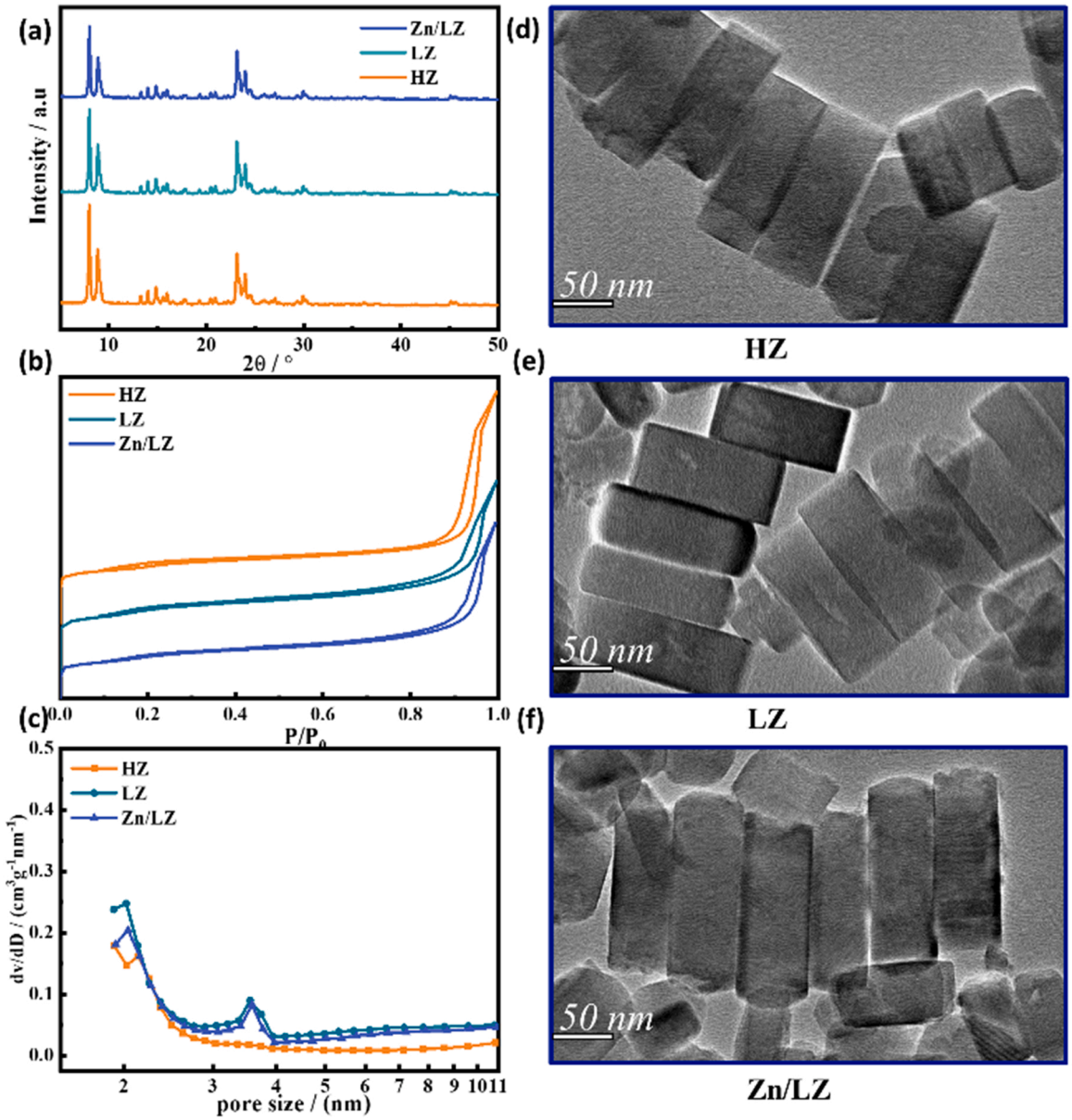

Fig. 3. (a) XRD patterns, (b) N_2-sorption isotherms, (c) pore size distribution and (d-f) representative TEM images of HZ, LZ, and Zn/LZ.

characterized by NH_3-TPD. As shown in Fig. 4a-b, the ammonia desorption peak areas of LZ were significantly larger than that of HZ, indicating a higher acid content of LZ than that of HZ (350 vs. 59 μmol g^{-1}, Table 2). After the introduction of Zn, the amount of strong acid of LZ signally reduced from 164 to 96 μmol g^{-1} of Zn/LZ, while the amount of weak acid was obviously increased from 76 to 125 μmol g^{-1}. And eventually, the total acid amount of Zn/LZ was slightly reduced to 343 μmol g^{-1} (Fig. 4c and Table 2). Meanwhile, the Brønsted acid sites were reduced from 47.3 μmol g^{-1} of LZ to 15.4 μmol g^{-1} of Zn/LZ, while the Lewis acid sites were increased from 27.5 to 39.2 μmol g^{-1} of Zn/LZ (Table 2). This was because that a lot of new Lewis acid sites, such as $[ZnOH]^+$ ions and $[ZnOZn]^+$ ions, were generated by the interaction of introduced Zn species and some original Brønsted acid sites of ZSM-5 zeolites [49]. In addition, because of the high Si/Al ratio, the amount of Brønsted acid sites and Lewis acid sites of HZ were only 10.5 μmol g^{-1} and 12.3 μmol g^{-1}, respectively.

Table 2
Acidic properties of HZ, LZ, and Zn/LZ samples.

Samples	NH_3-TPD (μmol g^{-1})				Py-IR (μmol g^{-1})		
	Weak	Medium	Strong	Total	Brønsted	Lewis	B/L
HZ	16	14	29	59	10.5	12.3	0.9
LZ	76	110	164	350	47.3	27.5	1.7
Zn/LZ	125	122	96	343	15.4	39.2	0.4

3.2. Inhibit deep alkylation of aromatics to increase catalytic stability

The methanol aromatization reaction was firstly carried out on single Zn/LZ bed (SL) and dual ZSM-5 bed (HZ & Zn/LZ, GU-1) respectively. Although the liquid hydrocarbons yield of SL could attain to 15.5 wt% during the first 10 h, it sharply reduced to 2.0 wt% in the second 10 h (Fig. 5a and b). Accompanied by this, the methanol conversion was also dramatically decreased from 99.7% to 81.2% within 20 h. By comparison, the catalyst lifetime of GU-1 was obviously prolonged to 75 h with a high liquid hydrocarbon yield of 12.1 wt%. Even after 75 h, the methanol conversion was still higher than 85%.

As for product selectivity, the aromatics selectivity of SL (42.6%) is significantly higher than that of GU-1 (24.3%, Fig. 5c). However, the most of aromatics in SL were trimethylbenzene and heavy aromatics with more than nine carbon atoms (C_{9+A}), which accounted for 29.6% and 18.5% in total aromatics, respectively. On the contrary, due to the pre-conversion of methanol on upper HZ catalyst bed, the deep alkylation of aromatics in GU-1 was signally inhibited. As shown in Fig. 5d, the light aromatics (BTX) became the main aromatic products with a relatively high selectivity of 67.1%, much higher than 50.0% of SL. And the selectivity of trimethylbenzene (TMB/A) and C_{9+} aromatics (C_{9+A}/A) in total aromatics were dramatically reduced to 14.0% and 14.4%, respectively. The decrease of heavy aromatic selectivity indicated that the formation of coke precursor in GU-1 was also suppressed because of the reduction of deep alkylation, which was also the main reason for its significantly longer catalytic lifetime than SL.

It is known that the alkylation of primary aromatics is closely correlated with the methanol concentration. In dual bed (GU-1), methanol was firstly converted into light hydrocarbons on the upper HZ catalyst with low acid density, then transformed into aromatics on the lower Zn/LZ catalyst with abundant Brønsted acid sites and Zn-Lewis acid sites [7]. So, the methanol concentration in lower Zn/LZ bed was observably reduced, which signally inhibited the aromatic alkylation and coke deposition. However, for SL, because of the high acid density of Zn/LZ, methanol could directly convert into aromatics at a faster rate. The quite high concentration of methanol strengthened the formation of heavy aromatics and coke precursors, which resulted in the relative low BTX selectivity and poor catalytic stability (Fig. 6).

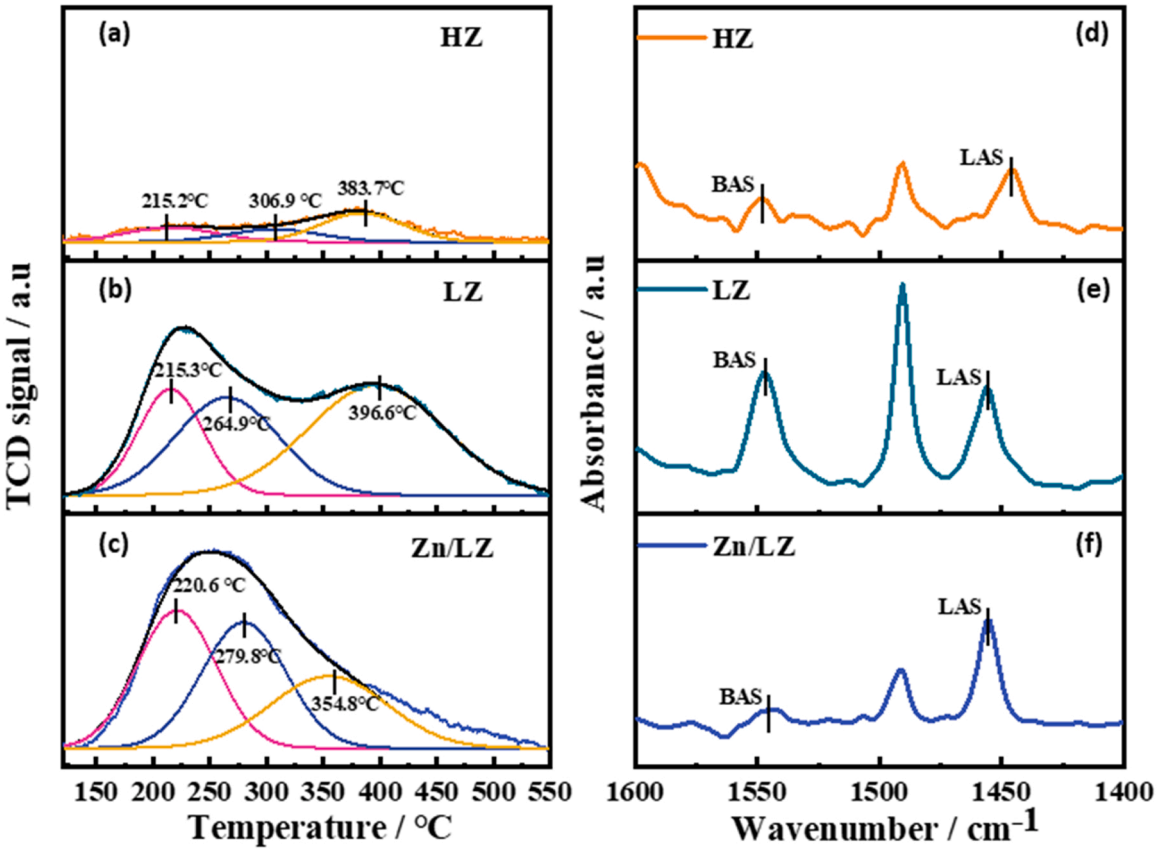

Fig. 4. (a-c) NH_3-TPD curves and (d-f) Py-IR spectra for the HZ, LZ and Zn/LZ respectively.

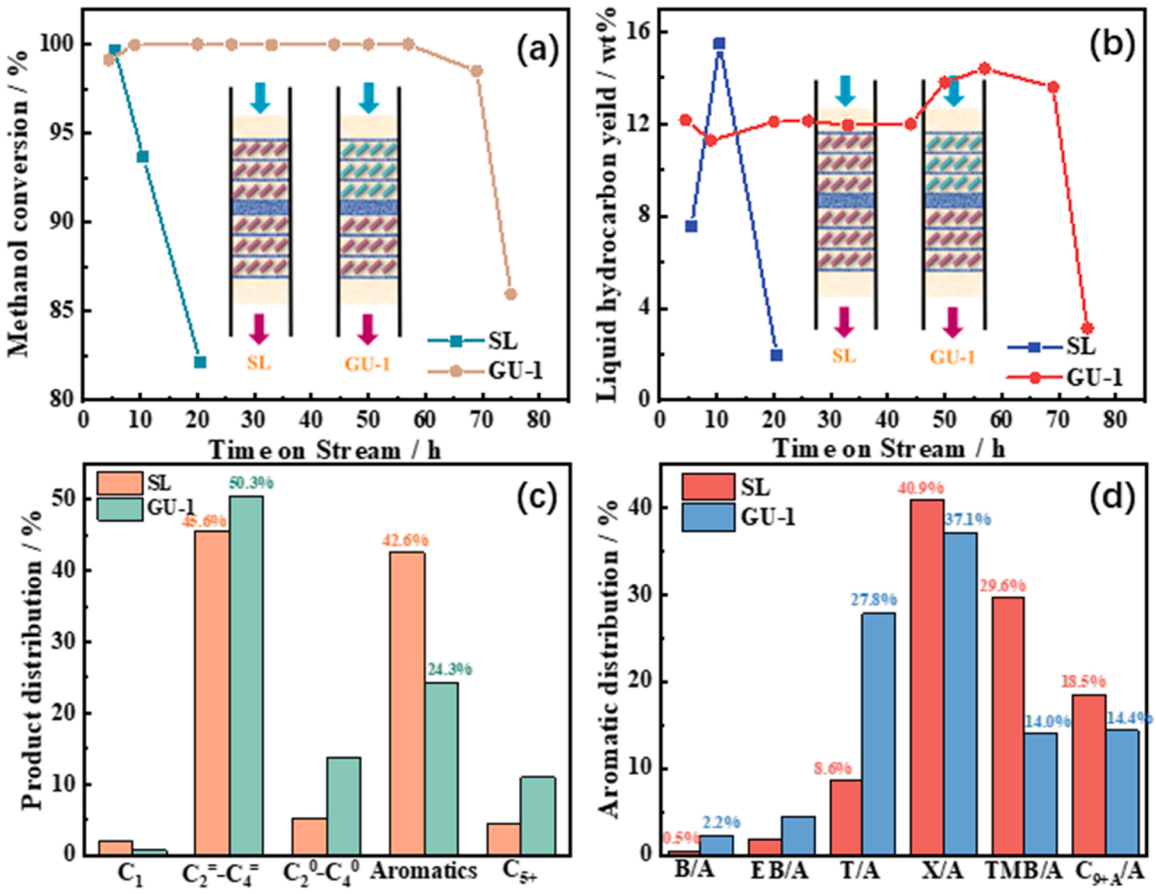

Fig. 5. (a) The methanol conversion, (b) liquid hydrocarbon yield, (c) the product distribution, and (d) the aromatic distribution of SL and GU-1 respectively.

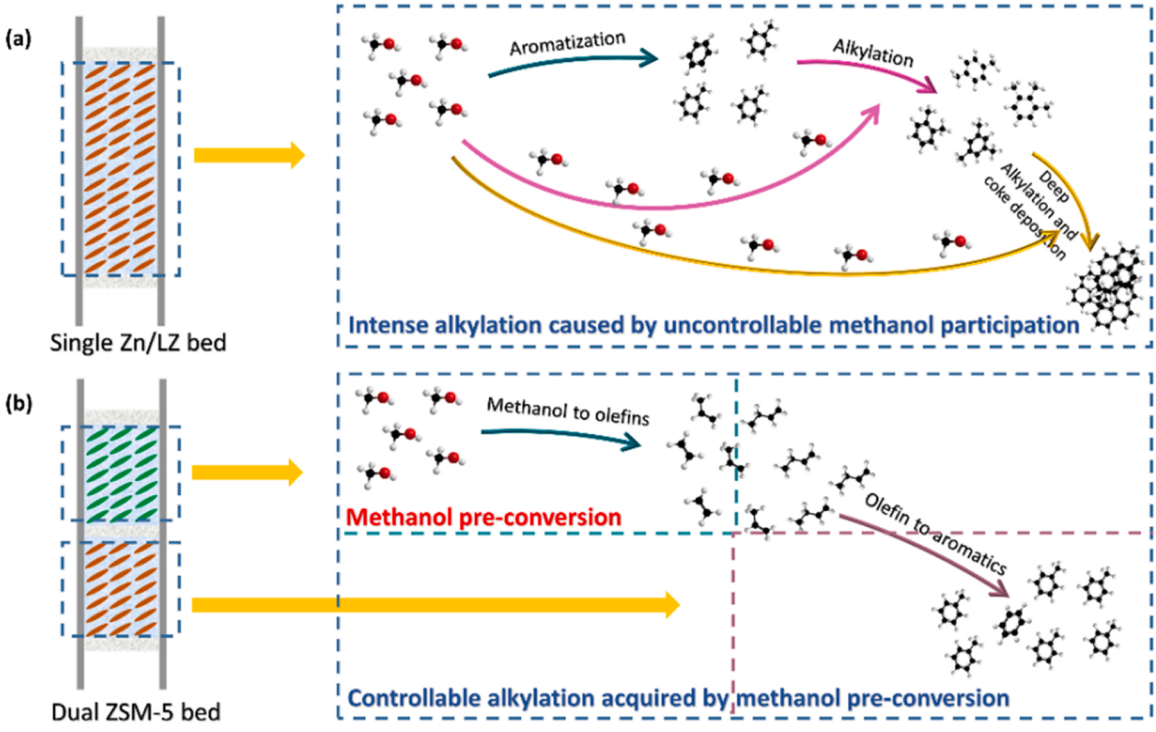

Fig. 6. Reaction path diagrams for MTA over single Zn/L bed (a) and dual ZSM-5 bed (b).

3.3. Precisely strengthen alkylation process to improve product selectivity

More importantly, although the catalytic stability was signally improved by suppressing the deep alkylation in GU-1, the low total aromatic selectivity (24.3%) and high toluene selectivity in total aromatics (27.8%) were undesired. Thus, the alkylation needed to be moderately enhanced in dual ZSM-5 bed to improve the aromatization performance and optimize product distribution. Unfortunately, regulating the methanol involvement in upper "methanol to olefins" to control the alkylation had a negligible effect on the final catalytic performance of dual catalyst bed (Figs. S1 and S2). But the gradually increased total aromatic selectivity and xylene selectivity as the reaction goes on (Figs. S3 and S4) indicated that enhancing the methanol concentration in the lower Zn/LZ catalyst bed was helpful to improve the aromatization of olefins and aromatic alkylation.

Thus, a part of methanol was directly introduced into the lower Zn/LZ catalyst bed to strengthen the alkylation for outstanding aromatization performance (Fig. 7). As shown in Fig. 8a, compared with that of GU-1, the liquid hydrocarbon yield was apparently enhanced from 12.1 to 13.9 wt% when partial methanol was introduced into the top of lower Zn/LZ catalyst bed (GL-1). And the liquid hydrocarbon yield could be further improved to 14.5 wt% and 16.3 wt% by reducing the methanol imported position to the middle and bottom of the lower Zn/LZ catalyst bed, respectively (GL-2 and GL-3, Fig. 8b-c). In addition, the catalyst lifetime of these dual beds was also extended as reducing the methanol-imported position, which was gradually prolonged from 81.0 h of GL-1 to 97.5 h of GL-2, and signally increased to 124.5 h for GL-3. The catalytic lifetime was significantly longer than those reported in most literatures for a single ZSM-5 bed (Table 3). However, when double methanol were introduced into the top of the lower Zn/LZ catalyst bed (DGL-1, Fig. 8d), the catalyst life was dramatically reduced to 45.0 h, although the liquid hydrocarbon yield was as high as 15.9 wt%.

As shown in Fig. 8e-h, the aromatic selectivity was significantly improved by introducing part of methanol into the lower Zn/LZ bed. Compared with 24.3% of GU-1, the aromatic selectivity in total products was increased to 38.1%, 40.2%, 35.0%, and 40.9% for GL-1, GL-2, GL-3, and DGL-1 respectively. Accordingly, the selectivity of light olefins in products was reduced from 50.3% of GU-1 to 38.3% of GL-1, 35.6% of GL-2 and 37.3% of GL-3, respectively, but increased to 40.8% for DGL-1.

For aromatic distribution (Fig. 8i-l), after introducing part of methanol into the top of Zn/LZ bed, the T/A was distinctly reduced from 27.8% of GU-1 to 23.6% of GL-1, which was further decreased to 20.9% and 13.1% as the methanol imported position reduced to the middle (GL-2) and bottom of Zn/LZ bed (GL-3), respectively. On the contrary, the X/A was apparently improved from 37.1% of GU-1 to 41.7% and 44.0% for GL-1 and GL-2 respectively, which was further increased to 46.0% for GL-3. Interestingly, the TMB/A slightly improved from 14.0% of GU-1 to 15.8% of GL-1 and 16.7% of GL-2, respectively, suggesting that the depth of alkylation was moderate in these two modes. However, the intense alkylation occurred when the methanol was introduced into the bottom layer of Zn/LZ bed. This was because that more aromatics were generated when the reactant moved toward the bottom of the catalyst bed, which provided more opportunities for direct alkylation of these aromatics with introduced methanol (Table S4). In this condition, TMB/A was dramatically improved to 21.6%. For DGL-1, the TMB/A was further increased to 26.3% accompanied by the decrease of X/A to 41.2%, which suggesting a more intense alkylation of aromatics as the increase of the amount of introduced methanol.

The trapped species in the Zn/LZ catalyst at 20 h in different modes were characterized by GC-MS (Fig. 9). By comparing Fig. 9a and b, it can be found that the GC-MS signals of methylbenzenes (trimethylbenzene, tetramethylbenzenes) of GL series were much higher than that of GU series, and gradually increased as the methanol imported position lowered (GL-1 to GL-3). These results were consistent with changes of product distribution, which suggested that alkylation of aromatics could be enhanced by introducing part of methanol into Zn/LZ catalyst bed and lowering the methanol imported position. Interestingly, although the alkylation was strengthened, the increase of large coke species like methylnaphthalenes was negligible in the GL series. However, the intensity of the signals of methylnaphthalenes was obviously enhanced when the double methanol were introduced (DGL-1), while the signal intensity of methylbenzenes, especially for tetramethylbenzene, were weakened (Fig. 9c). The signal distribution and strength of DGL-1 were similar to that of single methanol feeding mode (SL). The changes of these signals revealed that the excessive methanol inevitably caused the deep alkylation of aromatics, and further promoted the formation of coke during reaction process, which was the reason for the short catalytic lifetime of DGL-1. Above results illustrated that the moderate alkylation was necessary for the excellent catalytic performance of methanol aromatization for ZSM-5 catalysts.

3.4. Coke analysis of spent Zn/LZ catalysts under two feeding strategies

Fig. S10 presented the morphology features of spent Zn/LZ catalysts in GU-1 and GL series. Although the spent catalysts retained their original coffin shape, the edges became more blurred and uneven compared to that of fresh catalysts in Fig. 3f. In addition, the damaged cuboidal hollow carbon could be observed from the transmission electron microscope photographs (TEM) of 10 v% HF treated samples, which indicated that a large amount of coke species was deposited on the external surface of ZSM-5 catalyst (Fig. 10). Compared with that of GU-1, these phenomena on GL series were more prominent. The above

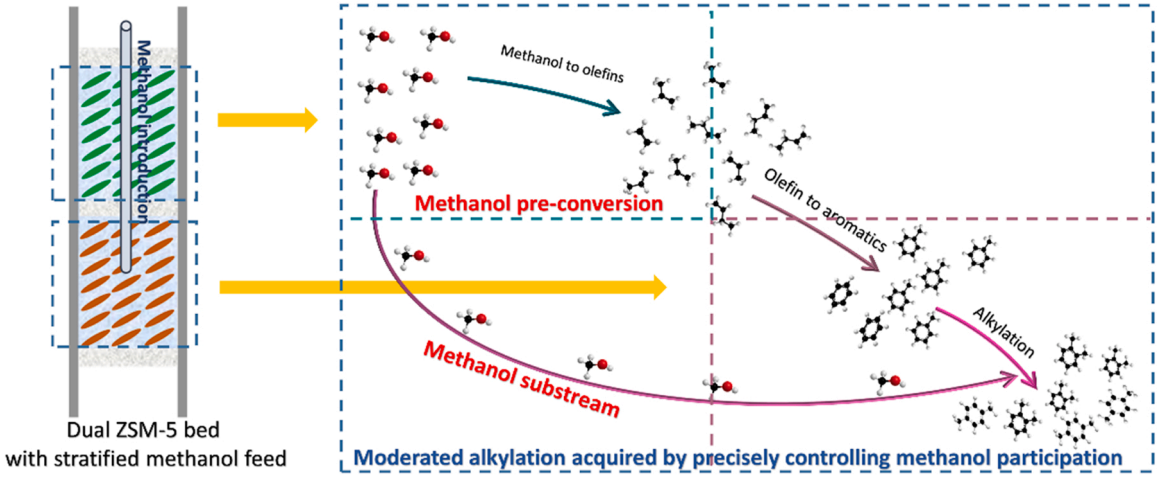

Fig. 7. Reaction path diagrams for MTA over dual ZSM-5 bed with stratified methanol feed (GL).

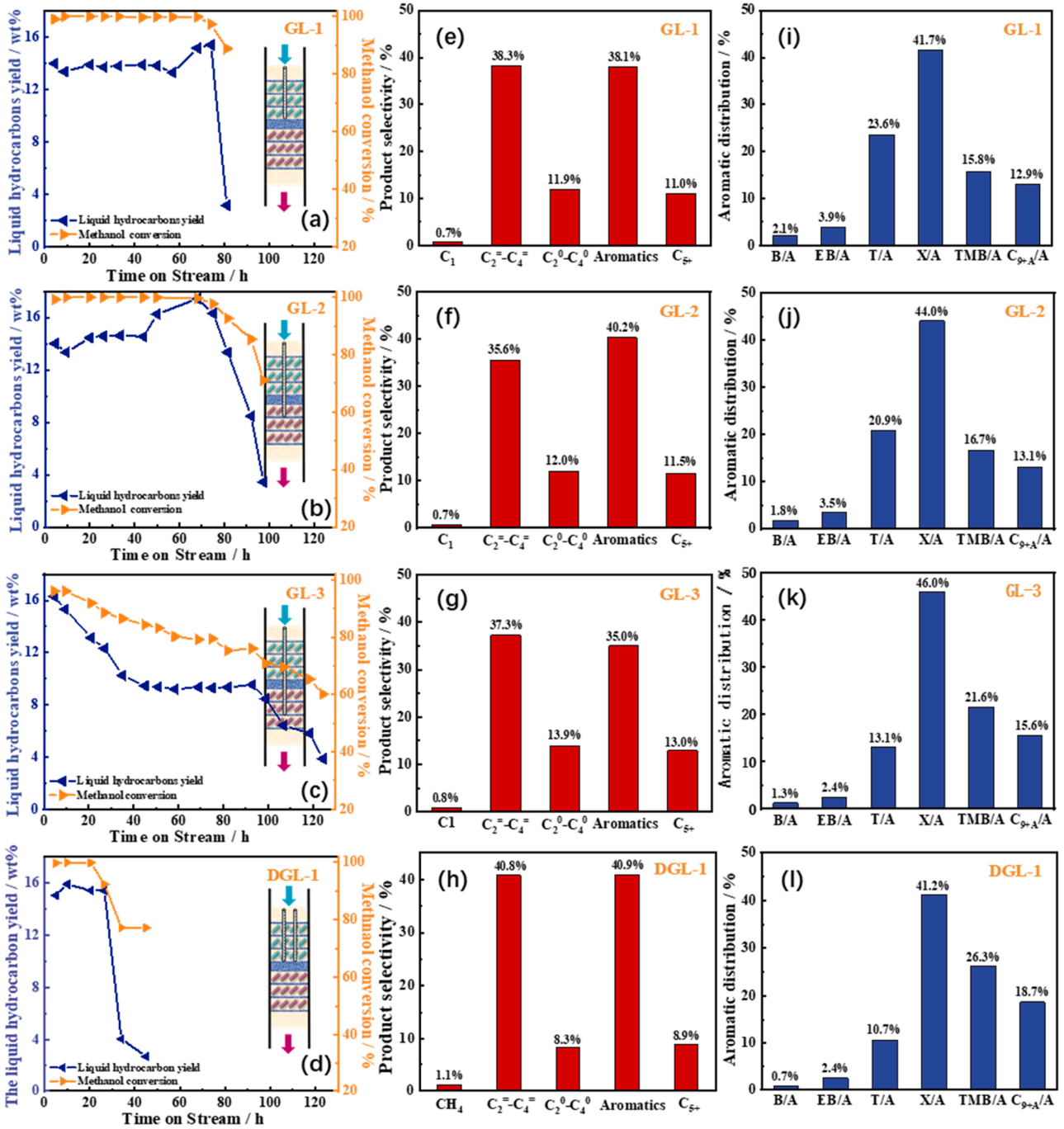

Fig. 8. Catalytic performances of GL-1 (a), GL-2 (b), GL-3 (c) and DGL-1 (d), the products selectivity and aromatic distribution for GL-1 (e, i), GL-2 (g, k), GL-3 (g, k) and DGL-1 (h, l), respectively.

observations indicated that the Zn/LZ catalysts in GU-1 and GL series had undergone a serious coke deposition process, especially for the methanol-introduced catalyst layers.

More detailed coke information was revealed by the thermal gravimeter analysis results (Fig. 11). As shown in Fig. 11a and b, the total coke amount on the top Zn/LZ catalyst layer in GL-1 was attained to 14.9 wt%. Along with the methanol-imported position moved down, the total coke amount of spent Zn/LZ catalyst were increased to 17.1 wt% of GL-2 and 22.1 wt% of GL-3 respectively, which were significantly higher than that of GU-1 (11.5 wt% for top layer, 9.5 wt% for middle layer and 8.2 wt% for bottom layer). Further comparing with that of GU-1, the amount of internal coke was obviously increased after introducing part of methanol into the lower Zn/LZ catalysts, which achieved to 73.2 mg g_{cat}^{-1} of GL-1 and 85.4 mg g_{cat}^{-1} of GL-2 and 109.8 mg g_{cat}^{-1} of GL-3 from 61.0 mg g_{cat}^{-1}, 48.8 mg g_{cat}^{-1} and 36.6 mg g_{cat}^{-1} of corresponding catalyst layer in GU-1 respectively (Fig. 11e and f). The significantly increased internal coke amount of GL series indicated that most of the introduced methanol could enter into the channel of ZSM-5 catalyst and participated in the aromatization process, even the formation of coke deposition. Because of this reason, most of the internal acid site could be utilized and expended. As the result, the residual acid amount of spent Zn/LZ catalysts apparently reduced from 0.10 mmol g^{-1} of top layer, 0.12 mmol g^{-1} of middle layer and 0.16 mmol g^{-1} of bottom layer in GU-1 to 0.09 mmol g^{-1} of top layer in GL-1, 0.04 mmol g^{-1} of middle layer in GL-2 and 0.02 mmol g^{-1} of bottom layer in GL-3, respectively (Fig. S8 and Table. S3). The full consumption of acid amount was also an

Table 3
Catalytic performance of ZSM-5 zeolite in the related researches.

Ref.	Catalysts	Lifetime	Aromatic selectivity	Reactor	Reaction conditions
[50]	3%Zn/ZSM-5(Si/Al=38)	–	25.0%	Fluidized bed	380 ℃, 0.4 MPa, WHSV= 0.3 h^{-1}
[34]	HZSM-5 (Si/Al=58, sheet)	50 h	25.7%	Fixed bed	475 ℃, 0.1 MPa, WHSV= 0.8 h^{-1}
[53]	HZSM-5 (Si/Al=90)	36 h	32.3%	Fixed bed	390 ℃, 0.5 MPa, WHSV= 3.2 h^{-1}
[52]	HZSM-5 (Si/Al=24)	40 h	33.8%	Fixed bed	450 ℃, WHSV= 2.3 h^{-1}
This work	HZSM-5 +Zn/ZSM-5 (Si/Al=250, 30)	97.5 h	40.2%	Fixed bed	450 °C, 0.1 MPa, WHSV= 4.0 h^{-1}
[37]	HZSM-5 (Si/Al=12)	–	44.6%	Fixed bed	475 ℃,0.1 MPa, WHSV= 0.79 h^{-1}
[18]	5%Zn/ZSM-5(Si/Al=36)	120 h	45.7%	Fixed bed	390 ℃, 0.5 MPa, WHSV= 3.2 h^{-1}
[51]	1%Zn/ZSM-5(Si/Al=25)	70 h	54.4%	Fixed bed	400 ℃, 0.1 MPa, WHSV= 1.5 h^{-1}

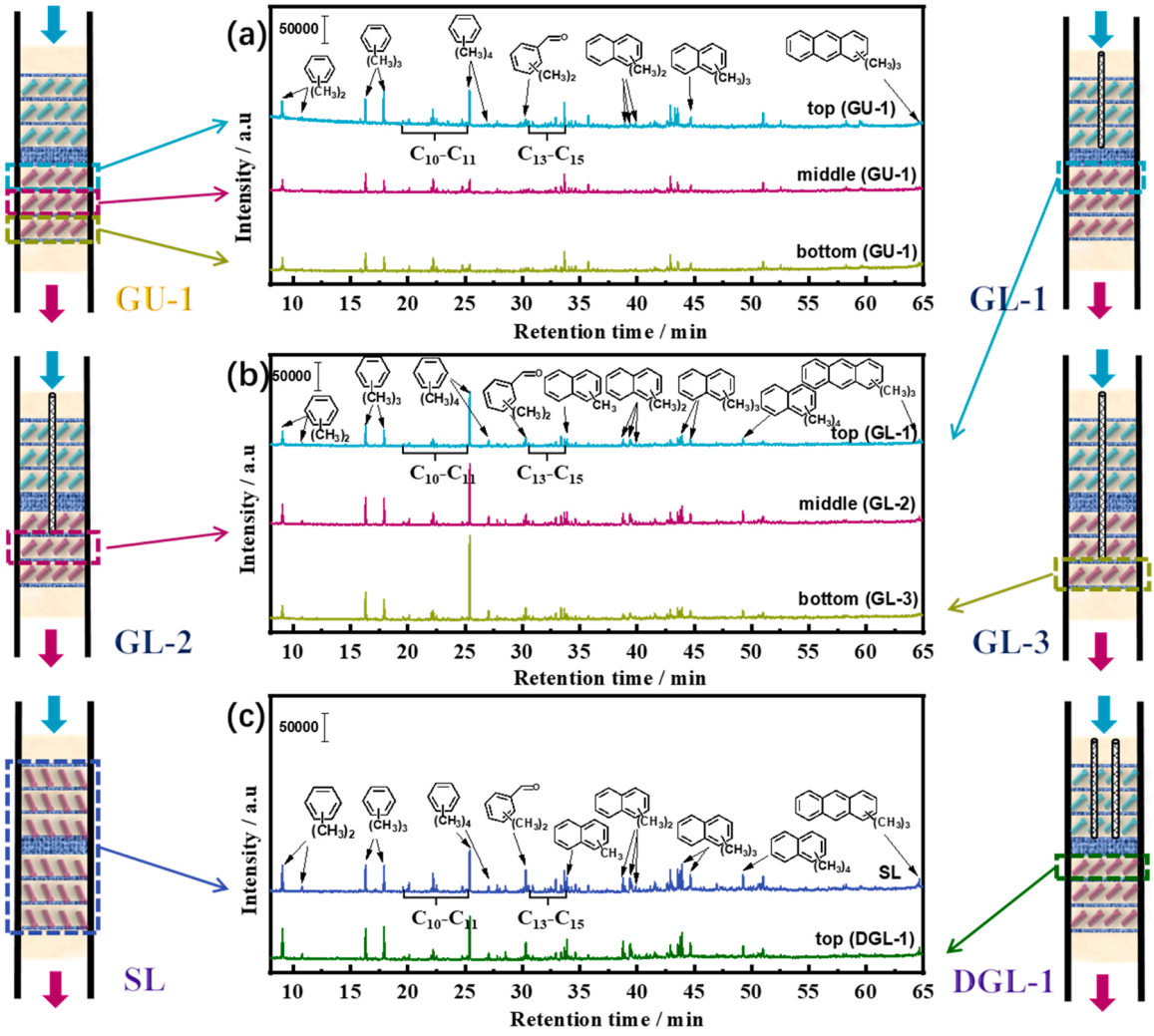

Fig. 9. GC-MS chromatograms of the organic extracts from the spent Zn/LZ catalysts in different modes and positions.

important factors for the excellent catalytic stability of GL series.

The soluble coke species remained in the micropore of spent Zn/LZ were extracted with CH_2Cl_2 after dissolving the zeolite framework by 10% of HF, and then recognized by GS-MS (Fig. 12). Obviously, alkylbenzenes, alkyl-naphthalenes and long-chain alkanes with more than ten carbon atoms were primary soluble coke species trapped in the spent Zn/LZ catalysts. Interestingly, the GC-MS signals of these soluble coke species were gradually weakened as the catalyst located position lowered in GU-1 mode (Fig. 12a), which was consistent with the results of TGA and NH_3-TPD of spent Zn/LZ catalysts. These results strongly reflected the underutilization of acid sites for Zn/LZ catalyst that located at the lower position of reactor in GU-1 mode.

After introducing part of methanol into the lower Zn/LZ catalyst layers (GL series), these GC-MS signals were dramatically enhanced

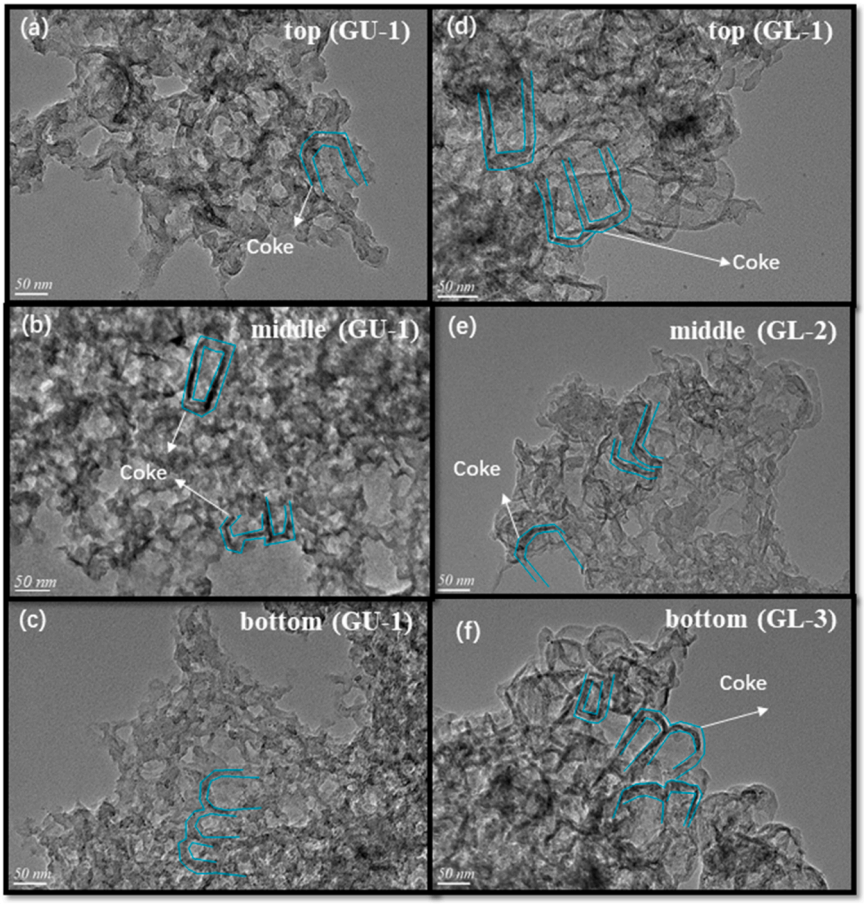

Fig. 10. TEM images of spent Zn/LZ catalysts treated by 10 v% HF in different position of GU-1 (a-c), GL-1 (d), GL-2 (e) and GL-3 (f) respectively.

comparing with that of GU-1 (Fig. 12b). The enhancement of the GC-MS signals suggested again that the aromatization process is enhanced by the introduction of methanol due to the enhancement of alkylation and the full utilization of internal acidic sites Zn/LZ catalysts. Thus, lots of soluble coke species remained in the micropores of the ultimate Zn/LZ catalysts.

3.5. Reaction scheme of the alkylation-controlled methanol aromatization

The DRIFT-TPSR technique was used to study the evolution of surface adsorbed species over Zn/LZ catalyst. Because propylene was the main component in light olefins formed in the upper HZ catalyst bed (accounting for more than 50%), both the methanol and propylene were chosen as the representative reactants for aromatization over the Zn/LZ catalyst. The DRIFT spectra were recorded at 350 ℃ with the reaction time increased from 1 to 60 min.

As shown in Fig. 13a-c, after feeding methanol for 2 min, the signals at 3740 cm^{-1} (attributed to external silanol groups, Si-OH) and 3600 cm^{-1} (corresponding to bridge hydroxyl groups, the Brønsted acid sites, Si(OH)Al) began to decline [54,55], while new peaks were appeared at 2955 cm^{-1}, 2924 cm^{-1}, 2871 cm^{-1}, 2855 cm^{-1} (assigned to the stretching vibration C-H bands in methyl groups) [56–58]. At the same time, a weak peak arosed at 1450 cm^{-1}, which was attributed to the C-H bending vibration of aromatic species [55]. All of these new generated infrared absorption peaks were became stronger as time goes on. These results showed that methanol molecules could rapidly absorbed on the hydroxyl sites of the ZSM-5 zeolite and disintegrated into the surface methyl species. The formation of aromatics was also rapid for methanol aromatization. It was worth noting that a large broad band visibly appears at 1585 cm^{-1} after 2 min, which was attributed to the C═C vibration in coke accumulation or pentamylbenzene and other macromolecular aromatic species [56]. The gradual increase of the peak intensity indicated that the obtained aromatic species during methanol aromatization were easily alkylated into polymethylbenzenes due to the existence of rich methyl species on zeolite surface. This result was consistent with the experimental evaluation.

For propylene feed, the introduced propylene molecule was mainly adsorbed on the Brønsted acid sites and gradually translated into olefinic cations, which could be confirmed by the enhanced bands of ν(CH) at 2964, 2937 and 2877 cm^{-1} and the decreased bands corresponded to the stretch bend of Si(OH)Al group at 3600 cm^{-1} after 5 min (Fig. 13d and e) [55,59]. After 7 min, dimethylcyclopentenyl cationic species (DMCP), the important intermediates for the formation of aromatics, were recognized by the new pick at 1510 cm^{-1} [59]. After 10 min, a weak peak at 1450 cm^{-1} (C-H bending vibration attributed to aromatic species) was appeared and gradually increased. Different with that of single methanol feed, the band at 1585 cm^{-1} attributed to the polymethylbenzenes was not appeared in the whole process (Fig. 13f). These signals revealed that propylene was preferentially transformed into dimethylcyclopentenyl cationic species, then further converted into aromatic species. However, because of the lack of alkylation reagent for propylene, it was difficult for aromatics to be deeply alkylated. Thus, no pick was fund at 1585 cm^{-1}.

When methanol was brought into the propylene stream by continuous bubble method, a large number of methyl species absorbed on the silanol groups and Brønsted acid sites (2955 cm^{-1}, 2924 cm^{-1} and 2855 cm^{-1}) were re-observed (Fig. 13g and h). These newly generated methyl species could provide sufficient raw materials for the alkylation of aromatics during propylene aromatization. As shown in Fig. 13i, in addition to the band at 1450 cm^{-1}, the band at 1585 cm^{-1} belonging to

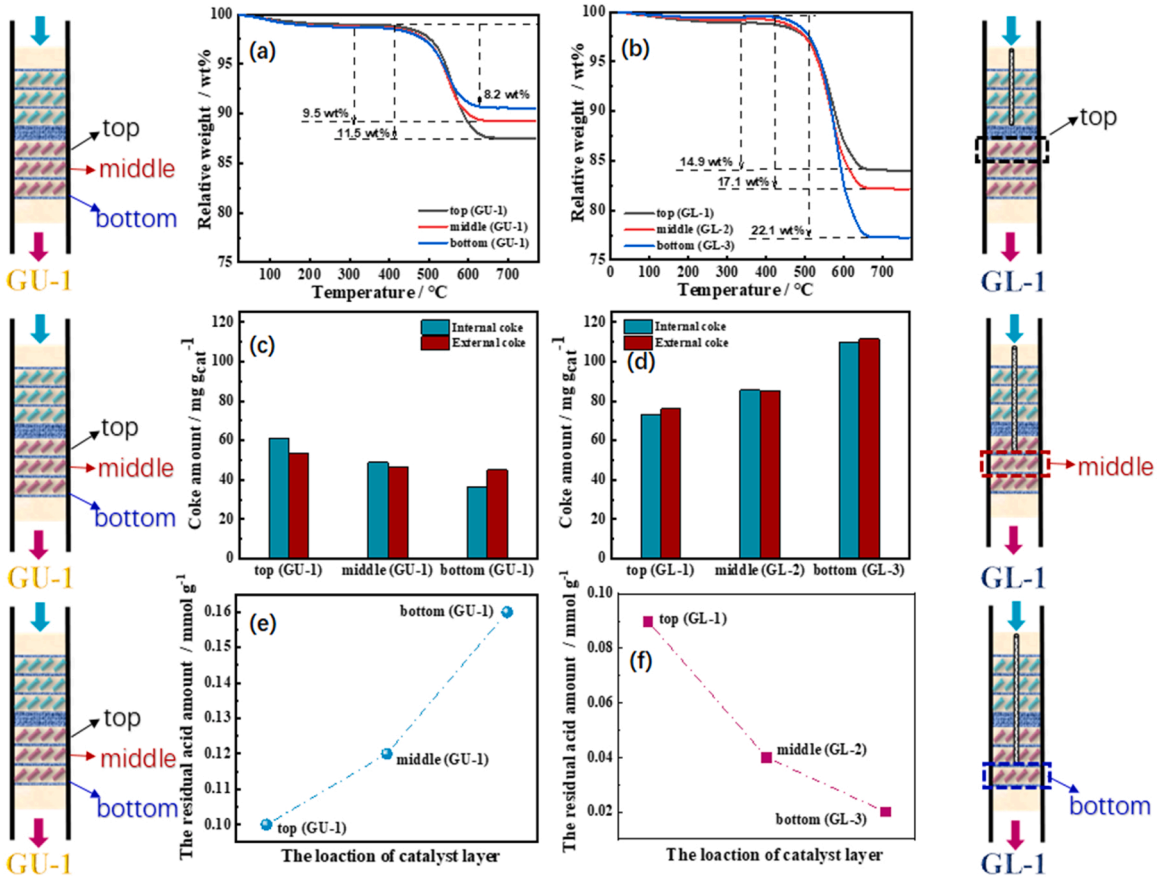

Fig. 11. (a) and (b) TG curves, (c) and (d) the distribution of coke deposition, (e) and (f) the residual acid amount for different spent Zn/LZ catalysts.

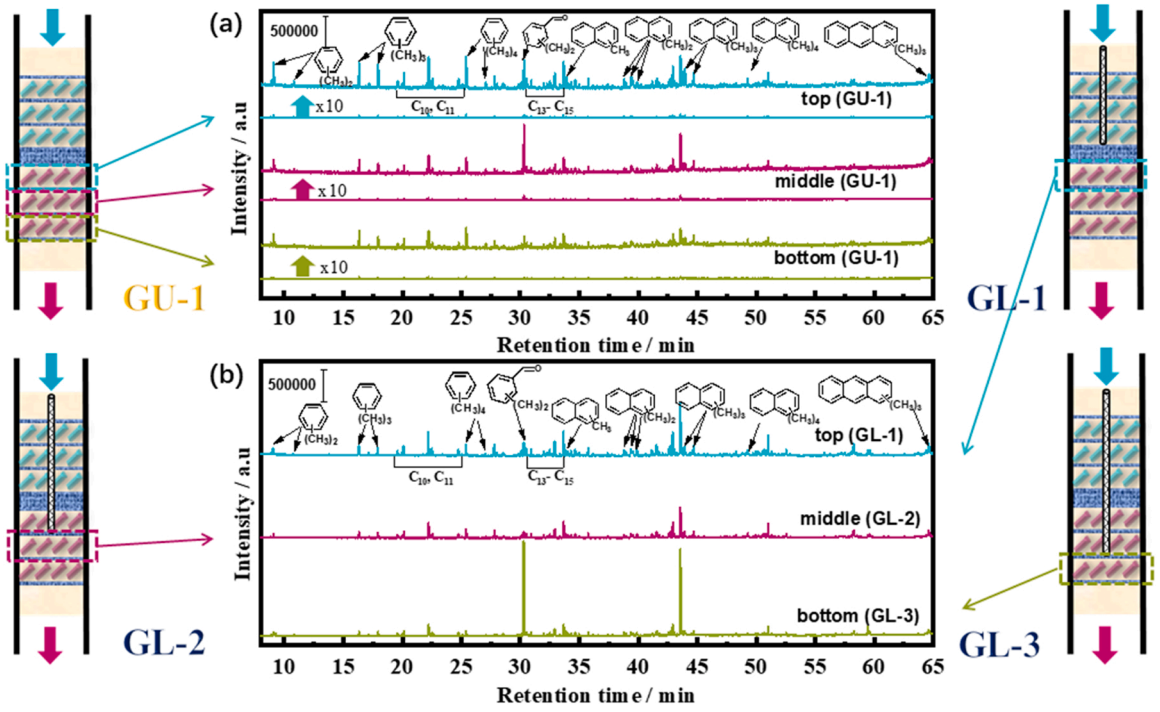

Fig. 12. GC-MS chromatograms of the soluble coke species from the inactivated Zn/LZ catalysts in different modes and positions.

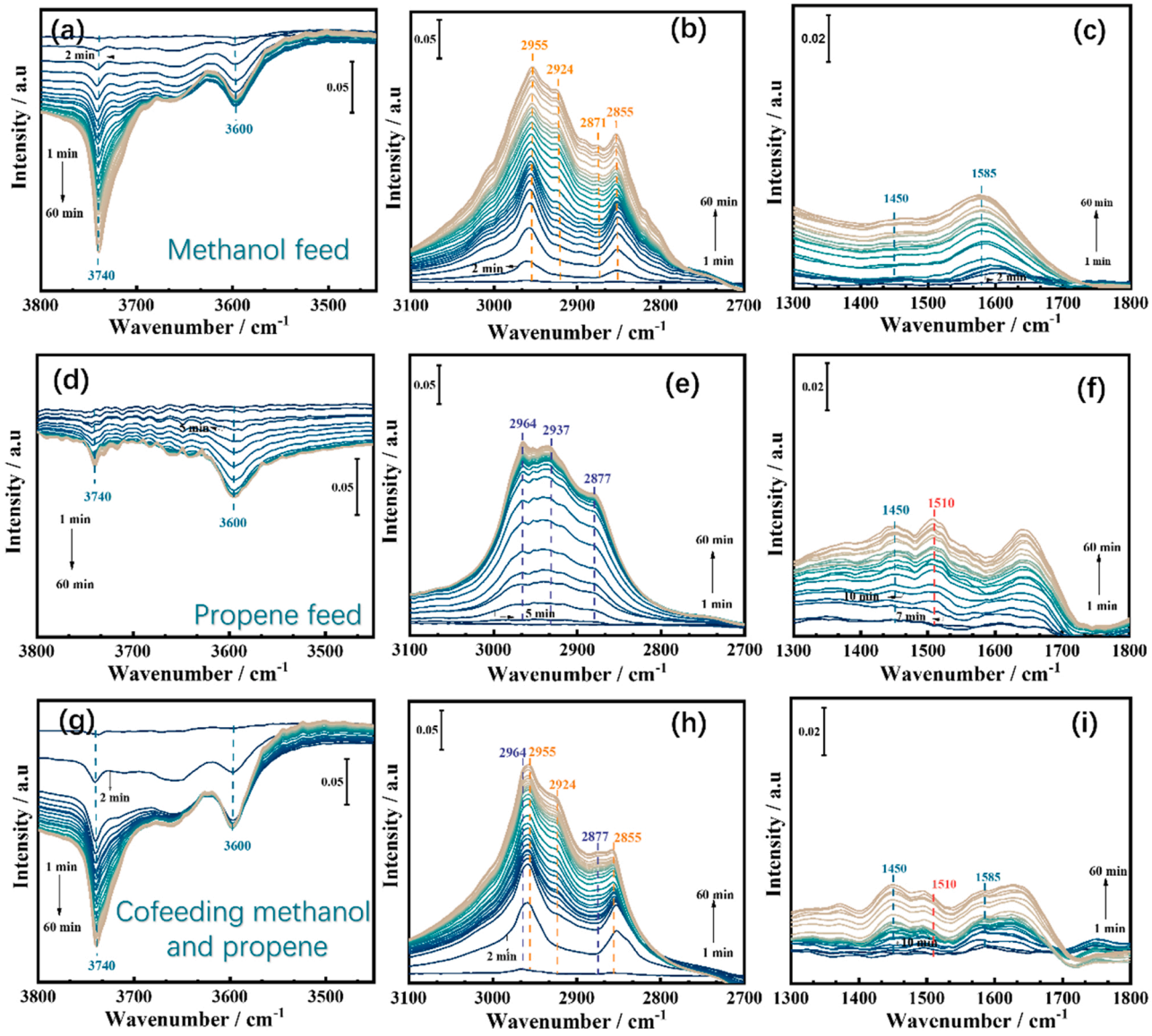

Fig. 13. In situ FT-IR spectra recorded as the time increased from 1 min to 60 min during methanol reaction (a-c), propylene reaction (d-f) and propylene-methanol reaction (g-i) over Zn/LZ catalysts at 350 °C.

the polymethylbenzenes were slightly increased after 10 min. However, the intensity of pick at 1585 cm^{-1} relative to that at 1450 cm^{-1} was much lower than that of single methanol reaction, suggesting a weaker alkylation of aromatics for propylene-methanol reaction. What's more, the intensity of the peak at 1510 cm^{-1} to that at 1450 cm^{-1} was also much lower than that of single propylene reaction. This result indicated that methanol could promote the conversion of DMCP to aromatics and indirectly promote the aromatization of propylene, which was the reason for the increase of aromatic selectivity of GL series. In addition to this, the in-situ measurements of cyclohexane-methanol also confirmed this conclusion (Figs. S14 and S15).

The positive effect of methanol on the aromatization of propylene was further confirmed by a series of temperature-programmed desorption experiments. The desorbed species were monitored by an on-line MS (Fig. 14). As the MS profiles of methanol desorption demonstrated in Fig. 14a, most of the unconverted methanol were desorbed when the desorption temperature was lower than 250 °C. In addition to the methanol, formaldehyde, acetaldehyde and methane were detected too, which indicated that methanol could be dehydrogenized and disproportionated under such temperature. Further increasing the desorption temperature above 300 °C, acetaldehyde and methane became the main desorption species. However, no signals of methylcyclopentene (MCP) and aromatics were detected.

For the temperature-programmed desorption of propylene, all of the desorption species were monitored at 250 °C. Expect the propylene, C_2-C_4 alkanes and hydrogen are the main desorption species, indicating that the hydrogen transfer reactions and dehydrogenation were easy to occur. What was noteworthy was that the clear signal of MCP (an important intermediate for aromatic) was also appeared at the same desorption temperature. No signal of aromatic was observed in all desorption species. These results indicated that propylene was more likely to produce MCP than methanol, but the further aromatization of MCP was hindered. Interestingly, by co-adsorption of propylene with trace amount of methanol, the signal of aromatics was monitored when the desorption temperature increased to 275 °C (Fig. 14c). This result confirmed that the aromatization of propylene/MCP could be promoted by introducing methanol.

Fig. 14d presented that the ratio of dimethyl-cyclopentene to methyl-cyclopentene in effluent was obviously increased by introducing the methanol into the olefin aromatization (GL-1 and DGL-1), which

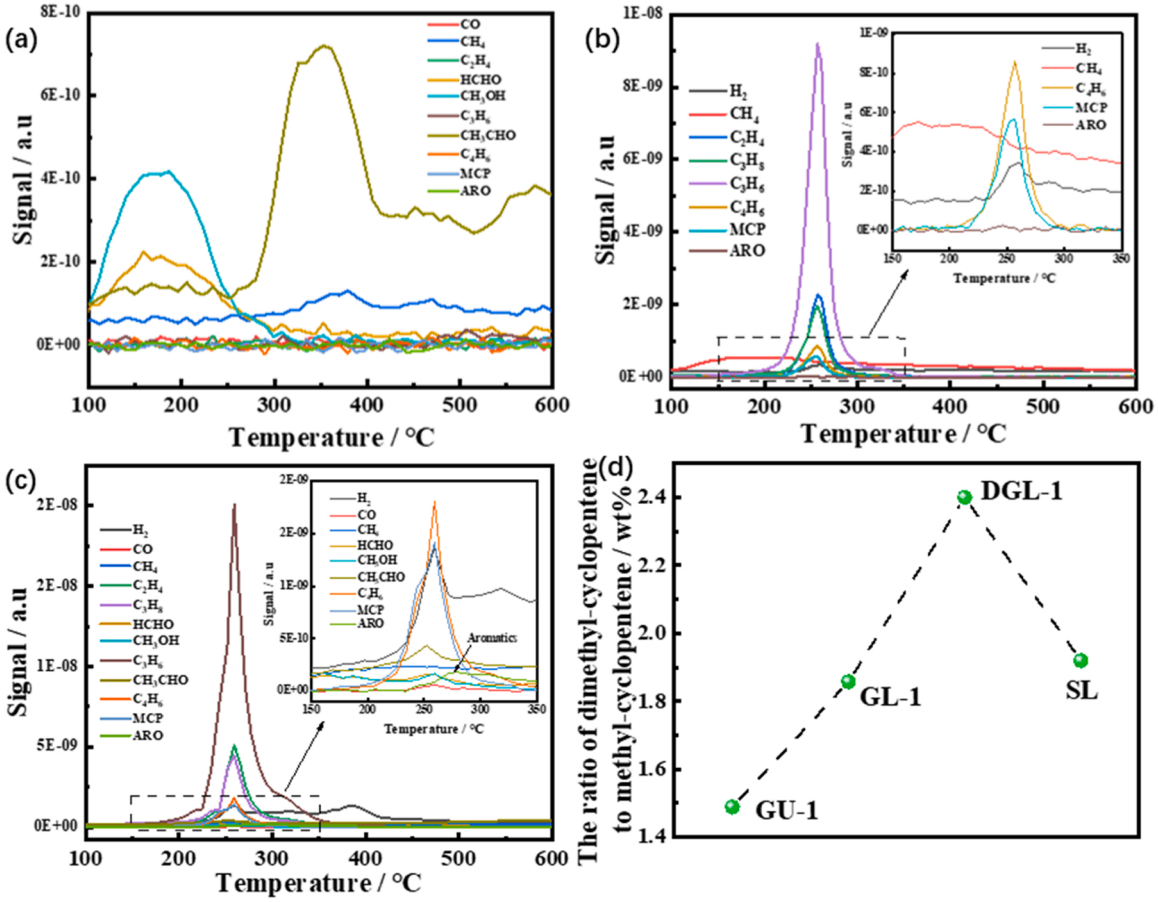

Fig. 14. Temperature-programmed desorption (TPD) of methanol (a), propylene (b) and the methanol-propylene mixtures (c) over Zn/LZ catalyst, the mass ratio of dimethyl-cyclopentene to methyl-cyclopentene in liquid products for GU-1, GL-1, DGL-1 and SL (d).

indicated a strengthened alkylation of MCP species. It is widely reported that the five-membered ring species, such as methylcyclopene, dimethylcyclopene, methylcyclopentenoneetc, can work as the critical intermediates for aromatic formation, and the initial aromatics could be generated by these five-membered ring species through alkylation, deprotonation, hydride transfer and ring expansion [60–63].

Enhancing the alkylation of MCP species is beneficial to aromatic production. Thus, it is easily to understand that although MCP species could be quickly formed from propylene via oligomerization, hydride transfer and cyclization, the lack of alkylation reagent required for the alkylation and ring expansion of MCP species delayed the generation of methylbenzenes. By injecting a part of methanol, the alkylation and ring expansion of MCP could apparently enhanced and methylbenzenes also could be readily produced by a series of methylation and dehydrogenation. And because of the relative scarcity of methanol, the deep alkylation of aromatics was significantly inhibited (Fig. 15). Therefore,

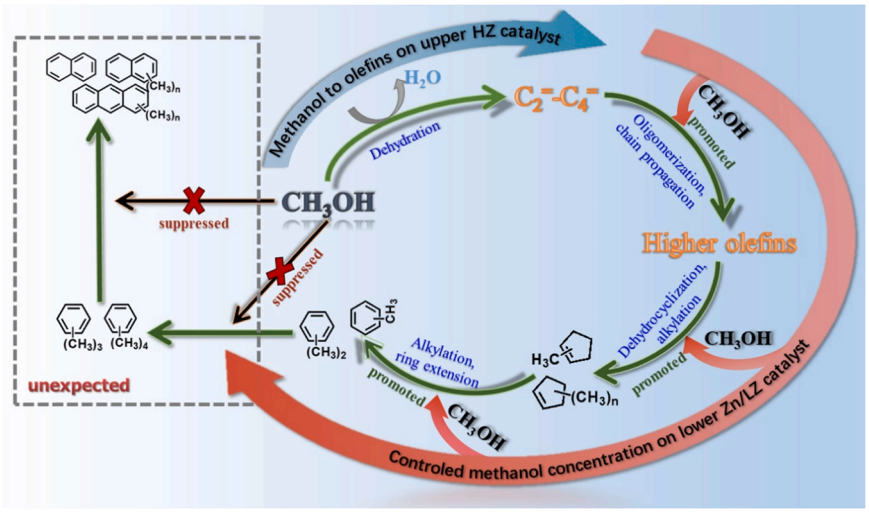

Fig. 15. The possible routes for methanol aromatization in dual ZSM-5 bed with controlled methanol concentration in lower Zn/LZ catalyst bed.

the aromatics selectivity and catalytic stability could be improved in the dual ZSM-5 bed with segmented methanol feed.

4. Conclusion

In summary, the alkylation reaction in MTA was accurately controlled by adjusting the distribution of methanol involvement using two strategies. One strategy was the pre-conversion of methanol into light olefins by packing high Si/Al ratio ZSM-5 (HZ) over the Zn doped low Si/Al ratio ZSM-5 (Zn/LZ) to inhibit the deep alkylation of aromatics and coke deposition. The other one was the introduction of part of methanol into the lower catalyst layers to strengthen the alkylation. The results revealed that the pre-conversion of methanol greatly prolonged the catalytic lifetime from 20 h of single Zn/LZ bed (SL) to 75 h of dual ZSM-5 bed (GU-1), and the light aromatic selectivity in total aromatics was also markedly enhanced from 50.0% to 67.1%. Introducing the methanol into the lower Zn/LZ bed mildly enhanced the alkylation, which apparently improved aromatization performance. After carefully regulating the imported position of methanol, the aromatic selectivity of the dual bed could signally increase from 24.3% of GU-1 to 40.2% of GL-2, and the catalytic life of GL-2 was extended to 97.5 h. The xylene selectivity in total aromatic products was also improved from 37.1% of GU-1 to 44.0% of GL-2, accompanied by the decrease of toluene selectivity from 27.9% to 20.8%. However, the excessive alkylation occurred when the methanol introduced position was reduced to the bottom of the lower Zn/LZ bed (GL-3) or the amount of introduced methanol was increased, which dramatically enhanced the trimethylbenzene selectivity from 14.0% of GU-1 to 21.6% and 26.2% of GL-3 and DGL-1 respectively. The results of coke analysis showed that introducing partial methanol into the lower Zn/LZ bed could promote the utilization of catalyst acid sites. The in situ experiments confirmed that the introduction of methanol can promote the conversion of olefins to aromatics by promoting the alkylation of methyl-cyclopentene. This work provides a new strategy to improve the production of high value-added aromatics and also provides a new understanding of the role of alkylation in MTA.

CRediT authorship contribution statement

Liangliang Zhang: Conceptualization, Investigation, Formal analysis, Validation, Data curation, Writing – original draft. **Tingjun Fu:** Conceptualization, Methodology, Writing – review & editing, Project administration, Funding acquisition. **Kun Ren:** Visualization, Data curation. **Yating Han:** Visualization. **Ran Wang:** Investigation, Validation. **Guowu Zhan:** Writing – review & editing, Conceptualization. **Zhong Li:** Supervision, Resources, Project administration, Funding acquisition.

Declaration of Competing Interest

The authors declare that they have no known competing financial interests or personal relationships that could have appeared to influence the work reported in this paper.

Acknowledgments

We thank the financial support from the National Natural Science Foundation of China (Nos. 21978191, 21878207), Key Research and Development Project of Shanxi Province (International Science and Technology Cooperation Program) (201803D421011).

Appendix A. Supplementary material

The Supporting Information is available free of charge at the online version of this article. Additional experimental results of the studied samples (Figs. S1-S15 and Tables S1-S4), including evaluation results, N_2-physisorption isotherms, NH_3-TPD, coke analysis, gas chromatography results, textural and acidic properties of spent catalysts.

Supplementary data associated with this article can be found in the online version at doi:10.1016/j.apcatb.2022.122047.

References

[1] T. Li, T. Shoinkhorova, J. Gascon, J. Ruiz-Martínez, Aromatics production via methanol-mediated transformation routes, ACS Catal. 11 (2021) 7780–7819.
[2] S. Kasipandi, J. Bae, Recent advances in direct synthesis of value-added aromatic chemicals from syngas by cascade reactions over bifunctional catalysts, Adv. Mater. 31 (2019), 1803390.
[3] Y. Ni, W. Zhu, Z. Liu, H-ZSM-5-catalyzed hydroacylation involved in the coupling of methanol and formaldehyde to aromatics, ACS Catal. 9 (2019) 11398–11403.
[4] D. Zhang, M. Yang, X. Feng, Y. Wang, Integration of methanol aromatization with light hydrocarbon aromatization toward increasing aromatic yields: conceptual process designs and comparative analysis, ACS Sustain. Chem. Eng. 8 (2020) 11376–11388.
[5] J. Wei, R. Yao, Q. Ge, D. Xu, C. Fang, J. Zhang, H. Xu, J. Sun, Precisely regulating Brønsted acid sites to promote the synthesis of light aromatics via CO_2 hydrogenation, Appl. Catal. B Environ. 283 (2021), 119684.
[6] Q. Roode-Gutzmer, D. Kaiser, M. Bertau, Renewable methanol synthesis, ChemBioEng Rev. 6 (2019) 209–236.
[7] T. Fu, J. Shao, Z. Li, Catalytic synergy between the low Si/Al ratio Zn/ZSM-5 and high Si/Al ratio HZSM-5 for high-performance methanol conversion to aromatics, Appl. Catal. B Environ. 291 (2021), 120098.
[8] J. Li, J. Xie, D. Zhang, L. Liu, J. Xing, Effect of alkali modification to ZSM-5 zeolite on the aromatization of methanol, J. Fuel Chem. Technol. 49 (2021) 339–346.
[9] H. Liu, H. Wang, A. Xing, J. Cheng, Effect of Al distribution in MFI framework channels on the catalytic performance of ethane and ethylene aromatization, J. Phys. Chem. C 123 (2019) 15637–15647.
[10] Y. Chai, W. Dai, G. Wu, N. Guan, L. Li, Confinement in a zeolite and zeolite catalysis, Acc. Chem. Res. 54 (2021) 2894–2904.
[11] U. Olsbye, S. Svelle, M. Bjorgen, P. Beato, T. Janssens, F. Joensen, S. Bordiga, K. Lillerud, Conversion of methanol to hydrocarbons: how zeolite cavity and pore size controls product selectivity, Angew. Chem. Int. Ed. Engl. 51 (2012) 5810–5831.
[12] Y. Ni, W. Zhu, Z. Liu, Formaldehyde intermediate participating in the conversion of methanol to aromatics over zinc modified H-ZSM-5, J. Energy Chem. 54 (2021) 174–178.
[13] L. Yang, C. Wang, W. Dai, G. Wu, N. Guan, L. Li, Progressive steps and catalytic cycles in methanol-to-hydrocarbons reaction over acidic zeolites, Fundam. Res. 2 (2022) 184–192.
[14] W. Wen, S. Yu, C. Zhou, H. Ma, Z. Zhou, C. Cao, J. Yang, M. Xu, F. Qi, G. Zhang, Y. Pan, Formation and fate of formaldehyde in methanol-to-hydrocarbon reaction: in situ synchrotron radiation photoionization mass spectrometry study, Angew. Chem. Int. Ed. Engl. 59 (2020) 4873–4878.
[15] P. Gao, J. Xu, G. Qi, C. Wang, Q. Wang, Y. Zhao, Y. Zhang, N. Feng, X. Zhao, J. Li, F. Deng, A mechanistic study of methanol-to-aromatics reaction over Ga-modified ZSM-5 zeolites: understanding the dehydrogenation process, ACS Catal. 8 (2018) 9809–9820.
[16] X. Zhu, J. Zhang, M. Cheng, G. Wang, M. Yu, C. Li, Methanol aromatization over Mg-P-modified [Zn,Al]ZSM-5 zeolites for efficient coproduction of para-xylene and light olefins, Ind. Eng. Chem. Res. 58 (2019) 19446–19455.
[17] H. Chen, Y. Wang, C. Sun, F. Gao, L. Sun, C. Wang, Z. Wang, X. Wang, Aggregates of nano-sized ZSM-5 crystals synthesized with template-free and alkali-treated seeds for improving the catalytic performance in MTP reaction, Catal. Commun. 100 (2017) 107–111.
[18] X. Niu, J. Gao, K. Wang, Q. Miao, M. Dong, G. Wang, W. Fan, Z. Qin, J. Wang, Influence of crystal size on the catalytic performance of H-ZSM-5 and Zn/H-ZSM-5 in the conversion of methanol to aromatics, Fuel Process. Technol. 157 (2017) 99–107.
[19] L. Xing, Z. Wei, Z. Wen, X. Zhu, MTA-catalytic study for methanol aromatization over hierarchical ZSM-5 zeolite synthesized by kaolin, Pet. Sci. Technol. 35 (2017) 2235–2240.
[20] Y. Jia, J. Wang, K. Zhang, G. Chen, Y. Yang, S. Liu, C. Ding, Y. Meng, P. Liu, Hierarchical ZSM-5 zeolite synthesized via dry gel conversion-steam assisted crystallization process and its application in aromatization of methanol, Powder Technol. 328 (2018) 415–429.
[21] J. Yang, K. Gong, D. Miao, F. Jiao, X. Pan, X. Meng, F. Xiao, X. Bao, Enhanced aromatic selectivity by the sheet-like ZSM-5 in syngas conversion, J. Energy Chem. 35 (2019) 44–48.
[22] N. Wang, Y. Hou, W. Sun, D. Cai, Z. Chen, L. Liu, B. Ge, L. Hu, W. Qian, F. Wei, Modulation of b-axis thickness within MFI zeolite: correlation with variation of product diffusion and coke distribution in the methanol-to-hydrocarbons conversion, Appl. Catal. B Environ. 243 (2019) 721–733.
[23] Y. Ma, N. Wang, W. Qian, Y. Wang, J. Zhang, F. Wei, Molded MFI nanocrystals as a highly active catalyst in a methanol-to-aromatics process, RSC Adv. 6 (2016) 81198–81202.
[24] Y. Gao, B. Zheng, G. Wu, F. Ma, C. Liu, Effect of the Si/Al ratio on the performance of hierarchical ZSM-5 zeolites for methanol aromatization, RSC Adv. 6 (2016) 83581–83588.

[25] Y. Zhang, S. Wu, X. Xu, H. Jiang, Ethane aromatization and evolution of carbon deposits over nanosized and microsized Zn/ZSM-5 catalysts, Catal. Sci. Technol. 10 (2020) 835–843.
[26] G. Zhang, T. Bai, T. Chen, W. Fan, X. Zhang, Conversion of methanol to light aromatics on Zn-modified Nano-HZSM-5 zeolite catalysts, Ind. Eng. Chem. Res. 53 (2014) 14932–14940.
[27] G. Xu, X. Zhu, A core-shell structured Zn/SiO_2@ZSM-5 catalyst: preparation and enhanced catalytic properties in methane co-aromatization with propane, Appl. Catal. B Environ. 293 (2021), 120241.
[28] H. Xiao, J. Zhang, P. Wang, Z. Zhang, Q. Zhang, H. Xie, G. Yang, Y. Han, Y. Tan, Mechanistic insight to acidity effects of Ga/HZSM-5 on its activity for propane aromatization, RSC Adv. 5 (2015) 92222–92233.
[29] W. Wannapakdee, D. Suttipat, P. Dugkhuntod, T. Yutthalekha, A. Thivasasith, P. Kidkhunthod, S. Nokbin, S. Pengpanich, J. Limtrakul, C. Wattanakit, Aromatization of C_5 hydrocarbons over Ga-modified hierarchical HZSM-5 nanosheets, Fuel 236 (2019) 1243–1253.
[30] Y. Jia, J. Wang, K. Zhang, W. Feng, S. Liu, C. Ding, P. Liu, Promoted effect of zinc-nickel bimetallic oxides supported on HZSM-5 catalysts in aromatization of methanol, J. Energy Chem. 26 (2017) 540–548.
[31] H. Ji, Q. Zhang, B. Wang, C. Li, H. Shan, Synergistic effect of nickel species and γ-alumina added to HZSM-5 on the methanol to aromatics, Catal. Lett. 144 (2014) 1860–1867.
[32] J. Zhang, X. Zhu, S. Zhang, M. Cheng, M. Yu, G. Wang, C. Li, Selective production of para-xylene and light olefins from methanol over the mesostructured Zn-Mg-P/ZSM-5 catalyst, Catal. Sci. Technol. 9 (2019) 316–326.
[33] J. Li, K. Tong, Z. Xi, Y. Yuan, Z. Hu, Z. Zhu, Highly-efficient conversion of methanol to p-xylene over shape-selective Mg-Zn-Si-HZSM-5 catalyst with fine modification of pore-opening and acidic properties, Catal. Sci. Technol. 6 (2016) 4802–4813.
[34] J. Zhang, L. Wang, Z. Wu, H. Wang, C. Wang, S. Han, F.-S. Xiao, Solvent-free synthesis of core-shell Zn/ZSM-5@silicalite-1 catalyst for selective conversion of methanol to BTX aromatics, Ind. Eng. Chem. Res. 58 (2019) 15453–15458.
[35] I. Hill, A. Malek, A. Bhan, Kinetics and mechanism of benzene, toluene, and xylene methylation over H-MFI, ACS Catal. 3 (2013) 1992–2001.
[36] S. Ilias, A. Bhan, The mechanism of aromatic dealkylation in methanol-to-hydrocarbons conversion on H-ZSM-5: what are the aromatic precursors to light olefins, J. Catal. 311 (2014) 6–16.
[37] W.Q.J. Zhang, C. Kong, F. Wei, Increasing para-xylene selectivity in making aromatics from methanol with a surface-modified Zn/P/ZSM-5 catalyst, ACS Catal. 5 (2015) 2982–2988.
[38] G. Zhang, X. Zhang, T. Bai, T. Chen, W. Fan, Coking kinetics and influence of reaction-regeneration on acidity, activity and deactivation of Zn/HZSM-5 catalyst during methanol aromatization, J. Energy Chem. 24 (2015) 108–118.
[39] B. Liu, D. Slocombe, M. AlKinany, H. AlMegren, J. Wang, J. Arden, A. Vai, S. Gonzalez-Cortes, T. Xiao, V. Kuznetsov, P.P. Edwards, Advances in the study of coke formation over zeolite catalysts in the methanol-to-hydrocarbon process, Appl. Petrochem. Res. 6 (2016) 209–215.
[40] Z. Chen, H. Wang, W. Song, Y. Hou, W. Qian, Decentralized methanol feed in a two-stage fluidized bed for process intensification of methanol to aromatics, Chem. Eng. Process. Process Intensif. 154 (2020), 108049.
[41] R. Qi, T. Fu, W. Wan, Z. Li, Pore fabrication of nano-ZSM-5 zeolite by internal desilication and its influence on the methanol to hydrocarbon reaction, Fuel Process. Technol. 155 (2017) 191–199.
[42] C. Emeis, Determination of integrated molai extinction coefficients for infrared absorption bands of pyridine absorbed on solid acid catalysts, J. Catal. 141 (1993) 347–354.
[43] A. Bonnin, Y. Pouilloux, V. Coupard, D. Uzio, L. Pinard, Deactivation mechanism and regeneration study of Zn/HZSM-5 catalyst in ethylene transformation, Appl. Catal. A Gen. 611 (2021), 117976.
[44] J. Kim, M. Choi, R. Ryoo, Effect of mesoporosity against the deactivation of MFI zeolite catalyst during the methanol-to-hydrocarbon conversion process, J. Catal. 269 (2010) 219–228.
[45] S. Lee, M. Choi, Unveiling coke formation mechanism in MFI zeolites during methanol-to-hydrocarbons conversion, J. Catal. 375 (2019) 183–192.
[46] L. Yang, T. Yan, C. Wang, W. Dai, G. Wu, M. Hunger, W. Fan, Z. Xie, N. Guan, L. Li, Role of acetaldehyde in the roadmap from initial carbon-carbon bonds to hydrocarbons during methanol conversion, ACS Catal. 9 (2019) 6491–6501.
[47] Y. Liu, S. Muller, D. Berger, J. Jelic, K. Reuter, M. Tonigold, M. Sanchez-Sanchez, J. A. Lercher, Formation mechanism of the first carbon-carbon bond and the first olefin in the methanol conversion into hydrocarbons, Angew. Chem. Int. Ed. Engl. 55 (2016) 5723–5726.
[48] C. Zhang, G. Kwak, Y. Lee, K. Jun, R. Gao, H. Park, S. Kim, J. Min, S. Kang, G. Guan, Light hydrocarbons to BTEX aromatics over Zn-modified hierarchical ZSM-5 combined with enhanced catalytic activity and stability, Microporous Mesoporous Mater. 284 (2019) 316–326.
[49] J. Gao, C. Wei, J. Wang, M.W. Fan, Evolution of Zn species on Zn/HZSM-5 catalyst under H_2 pretreated and its effect on ethylene aromatization, ChemCatChem 11 (2019) 1–12.
[50] T. Wang, X. Tang, X. Huang, W. Qian, Y. Cui, X. Hui, W. Yang, F. Wei, Conversion of methanol to aromatics in fluidized bed reactor, Catal. Today 233 (2014) 8–13.
[51] Z. Wei, L. Chen, Q. Cao, Z. Wen, Z. Zhou, Y. Xu, X. Zhu, Steamed Zn/ZSM-5 catalysts for improved methanol aromatization with high stability, Fuel Process. Technol. 162 (2017) 66–77.
[52] D. Pan, X. Song, X. Yang, L. Gao, R. Wei, J. Zhang, G. Xiao, Efficient and selective conversion of methanol to para-xylene over stable H[Zn,Al]ZSM-5/SiO_2 composite catalyst, Appl. Catal. A Gen. 557 (2018) 15–24.
[53] X. Niu, K. Wang, Y. Bai, Y. Du, Y. Chen, M. Dong, W. Fan, Selective formation of para-xylene by methanol aromatization over phosphorous modified ZSM-5 Zeolites, Catalysts 10 (2020) 484.
[54] X. Sharelle, M. Campbell, Russell F. Howe, Methanol to hydrocarbons: spectroscopic studies and the significance of extra-framework aluminium, Microporous Mesoporous Mater. 29 (1999) 91–108.
[55] E. Uslamin, H. Saito, N. Kosinov, E. Pidko, Y. Sekine, E. Hensen, Aromatization of ethylene over zeolite-based catalysts, Catal. Sci. Technol. 10 (2020) 2774–2785.
[56] M.Visur Saepurahman, U. Olsbye, M. Bjørgen, S. Svelle, In situ FT-IR mechanistic investigations of the zeolite catalyzed methylation of benzene with methanol: H-ZSM-5 versus H-beta, Top. Catal. 54 (2011) 1293–1301.
[57] G. Hou, T. Fu, X. Li, Q. Ma, Z. Li, Creation of silanol nests on HZSM-5 catalyst to boost the alkylation of toluene with methanol for PX synthesis, Appl. Catal. A Gen. 642 (2022).
[58] J. Liu, N. He, W. Zhou, L. Lin, G. Liu, C. Liu, J. Wang, Q. Xin, G. Xiong, H. Guo, Isobutane aromatization over a complete Lewis acid Zn/HZSM-5 zeolite catalyst: performance and mechanism, Catal. Sci. Technol. 8 (2018) 4018–4029.
[59] S. Lin, Y. Zhi, W. Chen, H. Li, W. Zhang, C. Lou, X. Wu, S. Zeng, S. Xu, J. Xiao, A. Zheng, Y. Wei, Z. Liu, Molecular routes of dynamic autocatalysis for methanol-to-hydrocarbons reaction, J. Am. Chem. Soc. 143 (2021) 12038–12052.
[60] M. Hu, C. Wang, X. Gao, Y. Chu, G. Qi, Q. Wang, G. Xu, J. Xu, F. Deng, Establishing a link between the dual cycles in methanol-to-olefins conversion on H-ZSM-5: aromatization of cycloalkenes, ACS Catal. 10 (2020) 4299–4305.
[61] D. McCann, D. Lesthaeghe, P. Kletnieks, D. Guenther, M. Hayman, V. Van Speybroeck, M. Waroquier, J. Haw, A complete catalytic cycle for supramolecular methanol-to-olefins conversion by linking theory with experiment, Angew. Chem. Int. Ed. Engl. 47 (2008) 5179–5182.
[62] W. Zhang, M. Zhang, S. Xu, S. Gao, Y. Wei, Z. Liu, Methylcyclopentenyl cations linking initial stage and highly efficient stage in methanol-to-hydrocarbon process, ACS Catal. 10 (2020) 4510–4516.
[63] W. Dai, C. Wang, M. Dyballa, G. Wu, N. Guan, L. Li, Z. Xie, M. Hunger, Understanding the early stages of the methanol-to-olefin conversion on H-SAPO-34, ACS Catal. 5 (2015) 317–326.